**UNIVERSITY OF TRENTO - Italy**

**Department of Industrial Engineering**

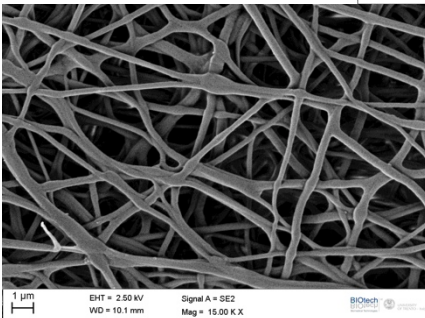**Doctoral School in Materials Science and Engineering**

# Single Polymer Micro- and Nano- Composites

## Thiago Medeiros Araujo





**April 2013**

# SINGLE POLYMER MICRO- AND NANO- COMPOSITES

## Thiago Medeiros Araujo

E-mail: thiago_medeiros@ymail.com

Approved by:

Prof. Alessandro Pegoretti, Advisor
Department of Industrial Engineering.
*University of Trento, Italy.*

Ph.D. Commission:

Prof. Paolo Scardi,
Department of Civil, Environmental
and Mechanical Engineering.
*University of Trento, Italy.*

Prof. Siegfried Schmauder,
Institute of Materials Testing,
Materials Science and Strength of
Materials (IMWF).
*University of Stuttgart, Germany.*

Prof. Chia-Kuang (Frank) Tsung,
Merkert Chemistry Center,
Department of Chemistry
*Boston College, USA.*

University of Trento, Italy.
Department of Industrial Engineering

April 2013

*To my Family*

# ABSTRACT

Due to an increasing attention to environment preservation and the need to accomplish new regulations, a general interest to improve the recyclability of composite materials has recently emerged. In order to fulfill this new requirements, a possible strategy could be represented by the development of so-called "single polymer composites" (SPCs), i.e. composite materials in which both matrix and reinforcement have the same chemical composition. The main advantage of SPCs is that, unlike traditional heterogeneous composites (such as glass- or carbon reinforced polymer composites), they can be entirely melted down at the end of the product life for recycling.

After an optimization of the annealing treatment to improve the mechanical properties and thermal stability of the reinforcing phase, SPCs containing Vectran® micro- and nano- fibers as a reinforcement were prepared, and their thermo-mechanical properties and recyclability were investigated using a multidisciplinary approach.

Single polymer micro composites (SPMCs) containing up to 30 wt% of reinforcing microfibers showed a outstanding improvement of tensile modulus (up to 160 %) compared with the unfilled matrix. FESEM observations evidenced some pull-out phenomena, indicating a poor interfacial adhesion. After a surface treatment on the reinforcement, a composite containing up to 20 wt% showed a remarkable improvement of almost 180% in the tensile modulus compared with the unfilled matrix. FTIR and thermal analysis evidenced its recyclability.

Single polymer nano composites (SPNCs) containing up to 10 vol% of reinforcing nanofibers showed an increase by almost 20% of their tensile modulus and strength in comparison with the unfilled matrix. Optical observations revealed a consolidation problem in the unfilled matrix due to the adapted film-stacking process used. However, the addition of the nanofibers in the composite eliminated the problem. Thermal analysis was used to ensure the SPNCs recyclability.

Vectran® single polymer micro- and nano- composites have been proven to be possible candidates to substitute traditional heterogeneous composites materials, with enhanced recyclability features.

# TABLE OF CONTENTS

# LIST OF FIGURES

IX

X

# LIST OF TABLES

# LIST OF ABBREVIATION AND ACRONYMS

| | |
|---|---|
| ATR | Attenuated total reflection |
| BP | 4,4'-biphenol |
| CIR | Crystallization induced reactions |
| DCM | Dichloromethane |
| DMTA | Dynamic mechanical thermal analysis |
| DSC | Differential scanning calorimetry |
| EEW | Epoxy equivalent weight |
| FESEM | Field emission scanning electron microscopy |
| FTIR | Fourier transform infrared |
| HBA | 4-hydroxybenzoic acid |
| HDPE | High density polyethylene |
| HNA | 6-hydroxy-2-naphthoic acid |
| LCA | Life cycle assessment |
| LCP | Liquid crystalline polymer |
| LDPE | Low density polyethylene |
| MPIA | Poly-m-phenylene isophthalamide |
| NPL | Non-periodic layer crystal (Model) |
| PA | Polyamide |
| PBI | Poly(2,2'-m-phenylene-5,5'-benzimidazole) |
| PBO | Poly-p-phenylene benzobisoxazole |
| PBT | Poly-p-phenylene benzobisthiazole |
| PCL | Para-crystalline lattices (Model) |
| PDLA | Poly-D-lactide |
| PE | Polyethylene |
| PEO | Poly(ethylene oxide) |
| PET | Polyethylene-terephthalate |
| PFP | Pentafluorophenol |
| PLA | Polylactic acid |
| PLLA | Poly-L-lactide |
| PMC | Polymeric matrix composites |
| PMMA | Polymethyl-methacrylate |

| | |
|---|---|
| PP | Polypropylene |
| PPTA | Poly-p-phenylene terephtalamide |
| PTFE | Polytetrafluoroethylene |
| SAED | Selected area electron diffraction |
| SPC | Single polymer composite |
| SPMC | Single polymer micro composite |
| SPNC | Single polymer nano composite |
| TA | Terephthalic acid |
| $T_{CN}$ | Crystallization temperature |
| TEM | Transmission electron microscopy |
| TGA | Thermo-gravimetric analysis |
| TLCP | Thermotropic liquid crystalline polymer |
| WAXD | Wide-angle X-ray diffraction |

# Chapter I

## INTRODUCTION

Fiber reinforced composites have been extensively studied since their creation in the beginning of the XX century. Fiber reinforced polymers have been widely used in several industries (e.g. automotive, aeronautical, aerospace) because of their particular mechanical and physical properties such as high specific strength and high specific stiffness.

Due to an increasing attention to environment preservation and the advent of the new regulations, a general interest to improve the recyclability of composite materials has recently emerged. In order to fulfill this new requirements, the development of so-called "single-polymer composites" (SPCs) is offered, in other words, composite materials in which both matrix and reinforcement have the same chemical composition. The main advantage of SPCs is that, unlike traditional heterogeneous composites (such as glass- or carbon reinforced polymer composites), they can be entirely melted down at the end of the product life for recycling. Besides recyclability, the interfacial bonding on SPCs should be improved based on the principle that matrix and fiber are made of the same polymer. A further driving force for SPCs is the possibility of manufacturing lightweight parts and structures because the density of SPCs is well below those of traditional filled polymers. The density of an equivalent composite is usually higher than that of an SPC because the former contain reinforcements such as glass (density: 2.5–2.9 $g/cm^3$), carbon (density: 1.7–1.9 $g/cm^3$), basalt (density: 2.7–3.0 $g/cm^3$), and fillers like talc (density: 2.7–2.8 $g/cm^3$), chalk (density: 1.1–2.5 $g/cm^3$) and silica (density: 2.1–2.6 $g/cm^3$). On the other hand, one of the main challenges in the SPCs production is the small melting temperature difference generally existing between a fiber and a matrix having the same chemical nature [1,2].

Liquid crystalline polymers (LCPs) represent a class of polymers well known for their excellent mechanical properties, thermal and chemical resistance, and low density, which result in remarkable specific properties [3]. Unlike conventional polymers, they crystallize from an ordered and oriented molecular phase intermediate between an isotropic liquid phase

and a crystalline solid, or amorphous glassy phase. Among the main uses of LCPs, the following applications should be mentioned: production of high precision moldings for use in the electronics industry, multi-way electrical connectors, components in printers and disk drives, transformer bobbins and encapsulation for surface-mounted silicon chips [4]. There are several commercial LCPs well known, that have been widely studied in the past decades between them Kevlar®, Twaron®, Zylon®, Ekonol®, Xydar® and Vectran® [3]. Vectran®, in particular, is superior to aramid fibers in several ways: it is highly resistant to creep, it resists flex or fold fatigue and abrasion, and it has better long-term resistance to UV degradation [4,5].

Previous investigations have shown that single-polymer composites can be successfully produced using commercially available continuous Vectran® fibers having different thermal transitions [6-8]. Also, heat treatments have been used to increase the mechanical properties and improve the thermal stability of LCP fibers [7,9-11].

When diameters of polymer fibers are reduced from micrometers to a few hundred nanometers, several attractive characteristics may be induced [12]. Some of the characteristics are a very large surface area to volume ratio (this ratio for nanofibers can be $10^3$ times larger than that of microfibers), flexibility in surface functionalities, change in crystalline structure [13], and superior mechanical performances (e.g. stiffness and tensile strength) [12]. All these characteristics with LCPs would open an avenue for applications in ultra-strong composites. There are several previous studies regarding nanofiber forming from LCPs [14-18]. On the other hand, to the best of our knowledge, there were no reports on forming Vectran® nanofibers.

Unlike conventional spinning methods, where the smallest diameters of tens micrometers can be achieved, the electrospinning technique can produce fibers with diameters ~10 nm to 1 mm [17,19-21]. In the electrospinning process, an electric field of elevated strength is applied to a needle through which polymer solution is delivered [17,19-21]. When the applied electric field overcomes surface tension and the viscoelastic forces in the droplet pendent or sessile at the needle exit, a charged jet of the polymer solution is ejected. The jet undergoes the electrically-driven bending instability which stretches it dramatically, while solvent evaporates [21]. As a result, solidified nanofibers are formed and are deposited on a solid collector, which is a grounded counter-electrode.

The aim of this work is to develop single-polymer composites (SPCs) using Vectran® micro- and nano- fibers and investigate their thermo-mechanical properties. Vectran® SPCs would open an avenue to substitute traditional heterogeneous composites in the automotive and aeronautical field, improving the lightweight of the final products and attending the newest regulations concerning the environment.

In chapter II the state of the art is reviewed, in the chapter III the materials and methods to produce Vectran® based SPCs are described, as well as the instrumentation used and thermal treatment procedure are detailed. In the subsequent chapter IV the main properties of the resulting composites are analyzed and discussed. In chapter V the conclusions are drawn.

# Chapter II

## BACKGROUND

### *2.1  Micro- and nano- composites*

Composite materials may be defined as materials made up of two or more components and consisting of two or more phases. Such materials must be heterogeneous at least on a microscopic scale. Fiber-reinforced composite materials consist of fibers of high strength and modulus, with dimensions on the order of microns, embedded in or bonded to a matrix with distinct interfaces between them. In this form, both fibers and matrix retain their physical and chemical identities, yet they produce a combination of properties that cannot be achieved with either of the constituents acting alone [22-25].

When at least one the reinforcement dimension is in the nanometer range (10 – 200 nm) the composite can be classified as nanocomposite. These composites show great promise not only in terms of superior mechanical properties, but also in terms of superior thermal, electrical, optical, and other properties. These characteristics are manifested, in general, at relatively low-reinforcement volume fractions. The principal reasons for such highly improved properties are; the properties of nano-reinforcements are considerably higher than the reinforcing fibers in use; and the ratio of their surface area to volume is very high, which provides a greater interfacial interaction with the matrix [22-25].

### 2.1.1  Single Polymer Composites

Although excellent mechanical properties have been achieved with, life cycle assessment (LCA) does not yield favorable results for ''traditionally'' reinforced composites. This is mostly due to the energy-intensive production of the reinforcements (e.g. glass, carbon, aramid fibers or fabrics) and limited recyclability of the corresponding composites. Glass fibers are the main component in polymeric matrix composites (PMCs), this kind of reinforcement is difficult to recycle both mechanically and thermally (incineration). In order to overcome this problem the natural fibers were

introduced as reinforcement, even if they are a renewable resource and can be thermally recycled, it is difficult to recycle then mechanically due to their poor thermal stability. This led to a search for alternative recycling-friendly homocomposites. Single polymer composites (SPCs) represent an effective alternative to the traditional fiber reinforced composites where the matrix and the reinforcement are from the same chemical composition, thereby supporting the ease of recyclability [2,26-28].

The new European Union directive on the end-of-life of vehicles (ELV 2000/53/EC), which states that by 2015 vehicles must be made of 95% recyclable materials, being 85% can be recovered through reuse or mechanical recycling and 10% through energy recovery or thermal recycling, lead the automotive industry to make every component recyclable [28].

Besides the recyclability there are other advantages in the use of SPCs: the possibility of manufacturing lightweight parts and structures in comparison with traditional composites due to lower density of polymeric fibers compared with traditional reinforcements (e.g. glass fiber, carbon fibers, basalt, talc, and silica); better interfacial adhesion fiber-matrix, in comparison with traditional composites, due to fully compatibility of them in the SPCs [2,27,28].

On the other hand, the main challenge in the SPCs production is the small difference, in terms of melting temperature, between matrix and reinforcement, once both constituents have the same chemical composition. This processing window can be expanded using polymers with same chemical composition but different chemical structure (e.g. HDPE and LDPE, PLLA and PDLA) or changing the chemical structure of the polymers [2,27].

In the 70s Porter et al. [29] introduced the concept and production of the SPCs using high density polyethylene (PE) as matrix and reinforcement. Later on, Ward [30-34] and his coworkers succeeded in the SPC production via hot compaction. Since then, several researchers started to study SPCs, not only with PE but several other polymers (e.g. polypropylene (PP) [35], polyethylene-terephtalate (PET) [36], polylactide acid (PLA) [37], polymethyl-methacrylate (PMMA) [38], Vectran® [6,7], polyamide (PA) [39], among others) [2,27,28].

Besides hot compaction it is possible to cite several SPC fabrication methods as: traditional melting, consists in a impregnation of the

reinforcement with a highly viscous matrix; overheating method, where the polymer fibers are overheated above their melting temperature when they are constrained, the constraining of the fibers increase their melting temperature offering the required temperature window; film-stacking, a textile reinforcement is sandwiched between matrix films and the material is produced by hot pressing; co-extrusion is used in order to generate SPC tapes; and *in-situ* polymerization [2,27,28].

If the single polymer composites using microfibers as reinforcement have been widely studied by the academia, the SPC containing nanofibers as reinforcement are not often studied. To the best of our knowledge, there is only one article in literature regarding the topic. Matabola et al. [40] studied the production and characterization of SPCs of PMMA containing nanofibers as reinforcement, it resulted in better dynamic mechanical properties in comparison with the PMMA matrix. This proves that SPCs using nanofibers can be the future in the field, improving not only mechanical properties, but inducing several kinds of functionalization to the final composite.

## 2.2    *Liquid crystalline polymers*

Reinitzer firstly observed liquid crystal state in the end of XIX Century, and together with Lehmann they started a new field, the liquid crystal science. In the beginning of the XX century Lehman, Friedel and Vorländer started to synthesize the first liquid crystalline compounds and established the existence of several types of liquid crystals [4,5].

In 1922 Friedel published a paper clearing the terminology of the liquid crystalline state and its different forms, nematic, smectic and mesophases. This nomenclature is still used nowadays. In the very next year Vorländer, studying the effect of increasing the length of liquid crystalline molecules, started to pursue the concept of a main-chain liquid crystalline polymer (LCP) [4,41]. In the 1960s DuPont achieved the first successful commercialization of LCPs with their aromatic amide fiber, spun from a lyotropic solution, under trade name of Kevlar®. For several years efforts to produce main-chain LCP stable without the addition of the solvents were frustrated due to the increase of the crystal melting point of rigid-chains crystals with increasing their chain length. The synthesis of rigid random copolymers of aromatic polyester (thermotropic LCP) by Jackson in the 70s

managed to reduce the melting point of LCPs, in this way it could be processed from molten state without suffering degradation [4]. Thermotropic main-chain LCPs have a unique integration of properties from both the liquid crystalline and the conventional thermoplastic states, such as melt processability, high mechanical properties, low moisture uptake, and excellent thermal and chemical resistance. The LCPs successful development and the recognition of their unique properties are the result of comprehensive research that has been carried out by both academia and industry over the past decades [4,5,42].

### 2.2.1 Classification and physical structure of liquid crystalline polymers

As mentioned before, LCPs can be classified as lyotropic or thermotropic depending on whether the liquid crystalline state is achieved in a solution or by increasing the temperature.

In the thermotropic LCPs, a purely thermal process induces the transition to the liquid crystal state. Thermotropic LCPs form thermally activated mesogenic phases that extend from the crystal melting temperature, $T_m$, up to the isotropic temperature, $T_i$, in other words, the liquid crystalline phase only exists between $T_m$ and $T_i$. Over the latter, the liquid crystalline phase reverts to an isotropic liquid. A liquid crystalline system in which transition temperatures are brought down by the addition of a low molecular weight solvent is known as lyotropic. Lyotropic solutions enable very rigid molecules to be handled, although wet processes have their own particular inconveniences and limitations [3-5,42,43].

As it can be seen in figure 1, in the crystal state there is a long-range order in position and orientation, while in the liquid state there is no long range ordering in either of them. The liquid crystalline state is a kind of state whose order is between the crystal solid and isotropic liquid states [3-5].

(a)          (b)          (c)
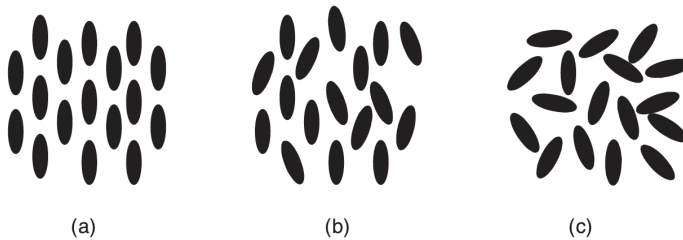
**Figure 1 –** The schematics of a) crystal state, b) liquid crystalline state and c) liquid state [5].

The liquid crystalline state can present several different structures between the amorphous isotropic structure and the perfect organized crystal and they are mainly classified in three different phases: nematics, smectics and cholesteric [41].

The nematics phase (N phase), are characterized by the non-presence of long-range translational order, but a long-range orientational order only. The molecules in it are aligned with respect to the vector known as the director ($n$). The quality of the alignment is not perfect, and is quantified by what is known as the order parameter (*S) [4,5,41,42]*. Nematics are the most important member in the family of the liquid crystals and are widely used in the display industry and its molecular organization is presented in figure 2 [5].
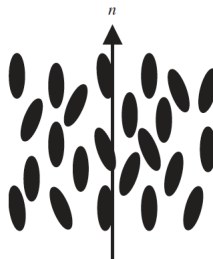


**Figure 2 –** The nematic phase [5].

In addition to the orientational order that the nematic phase shows, the smectic *A* and *C* phases exhibit a one-dimensional translational order, and can therefore form layered structures. In a smectic *A* phase the director lies along the layer normal. The molecular packing within the layers is liquid-like

and has no long- range positional correlation. Likewise, there is no correlation between the lateral positions of the molecules in successive layers. Because of the disorder within the layers, the layers are not well defined, and in formal terms the smectic *A* can be described as a one-dimensional density wave. As in a nematic, the alignment of the molecules with the director is not perfect and is described by *S*. The smectic *C* only differs from smectic *A* because the director of each layer is inclined at an angle $\omega$ to the layer normal, this angle remain the same for all layers [4,5]. They are schematically showed in figure 3.
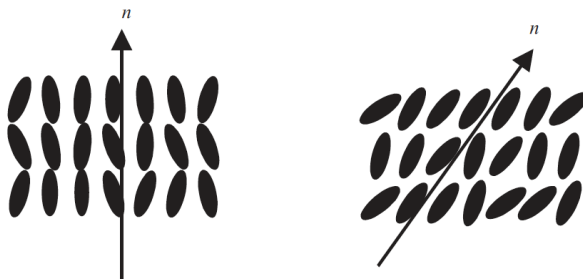


**Figure 3 –** The smectic *A* and *C* phases, respectively [5].

The cholesteric phase is equivalent to a nematic that has been twisted periodically about an axis perpendicular to the director. The twist in a cholesteric phase arises spontaneously when the mesogenic molecules have a chiral nature. However, it is possible to induce the cholesteric phase formation introducing chiral elements in the polymer or, introducing a chiral component with low molecular weight in the nematic polymer. The molecules in cholesteric liquid crystals are arranged as thin layers. The molecules lie in the layers and are parallel to each other, but the director rotates along the helical axis continuously and uniformly. The helical pitch is much greater than the spacing of successive molecular layers, as schematically represented in figure 4 [4,5,42].
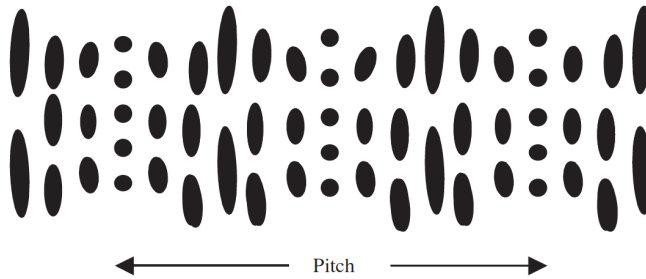
**Figure 4 –** The cholesteric phase [5].

Several other crystalline phases exists (e.g. cubic, hexagonal, lamellar, columnar), since they are not frequently present in thermotropic liquid crystals, they will not be further detailed.

### 2.2.2    Classification and chemical structure of liquid crystalline polymers

The LCPs can be classified not only as thermotropic and lyotropic, but also in function of their molecular geometry and the nature of the mesogenic functional groups inside the polymeric chain. According to the way the mesogenic units are incorporated into the polymers, the liquid crystalline polymers can be classified as main-chain liquid crystalline polymers in which the mesogenic units are connected in the backbone, or side-chain liquid crystalline polymers in which the mesogenic units are attached to the backbone as side pendants. Both examples can be seen on figure 5.
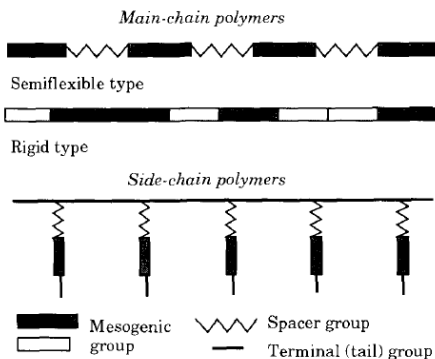
Figure 5 – Examples of main-chain and side-chain liquid crystalline polymers [44].

Mesogenic units give to the LCPs their anisotropic rod shape, it must be essentially linear and of high aspect ratio. The typical mesogenic group consists of at least two aromatic or cycloaliphatic ring connected in the *para* positions by a short rigid link, which maintains the linear alignment of the rings. At first it was believed that the mesogenic group should be completely inflexible. However, it was revealed lately that the mesogenic group might contain a flexible sub-unit [44].

Most main-chain LCPs are composed of mesogenic units linked by spacers with different degrees of flexibility (e.g. methylene, oxyethylene, siloxane groups), in order to reduce the mesomorphic temperature of liquid crystalline polymers and increase their processability. The participation of flexible spacers dramatically changes the properties of liquid crystalline polymers. These properties depend not only on the mesogenic units but also on the type of flexible spacers. However, some main-chain LCPs, like Vectran, are fully aromatic and no flexible chain group is present. The required lowering of the transition temperature, in this case, is accomplished with a copolymerization of 2,6-naphthalene units in the main chain [4,5,44].

The side-chain LCPs similar to the main-chain LCPs use some flexible units as spacer groups. Attached to each mesogenic group is a terminal group, normally being –OR, –R, –CN, –H, –NO$_2$, –NH$_2$, –Cl and –Br [5,44].

### 2.2.3    Liquid crystalline polymer fibers

Both lyotropic and thermotropic LCPs are currently used for fiber production and they are probably the ideal precursors for preparing it. In the both, solution or molten, states the degree of uniaxial orientation is typically very high and the extensional flow that is associated with the extrusion process orients the mesophases in the flow direction. Exploiting the anisotropy of LCPs a very high orientation can be reached during the fiber production, which means outstanding tensile mechanical properties coupled with low density resulting in very good specific properties [3].

Nowadays LCP fibers are divided mainly in three classes: aromatic polyamides, aromatic heterocycles and aromatic copolyesters. The first one is commonly known as aramid fibers, they are obtained from polyamides containing aromatic rings along the main chain. Typically the aromatic units are phenylene or naphthalene rings and they present a rod-like behavior. These fibers cannot be produced by melt-spinning because they decompose before reaching the melting temperature, and in this case they are generally obtained from polymer solutions being a lyotropic LCP. As main applications it is possible to cite; advanced fabrics, coatings, and fillers, advanced composites in the aerospace and armament industry, asbestos substitutes, electrical insulation, bullet-proof body armor, industrial filters, and protective and sport clothing [45]. Their most known commercial products are; Kevlar® (Dupont, USA) and Twaron® (Teijin Aramid, Japan), both based on poly-*p*-phenylene terephthalamide (PPTA); Nomex® (Dupont, USA) and Tijinconex® (Teijin Aramid, Japan), poly-*m*-phenylene isophthalamide (MPIA) based; Technora® (Teijin Aramid, Japan) based on 3,4'-POP-T copolymer [3].

The aromatic heterocycles, like the aromatic polyamides, present lyotropic behavior. They are characterized by a wholly aromatic molecular structure with fused heterocyclic rings along the main-chain. Poly(*p*-phenylene benzobisthiazole) (PBT) and poly(*p*-phenylene benzobisoxazole) (PBO) are the most diffused within this class, both can be spun into fibers with mechanical properties even superior to that of aromatic polyamides fibers, the latter is commercialized under tradename of Zylon® (Toyobo, Japan). On the other hand, Poly(2,2'-*m*-phenylene-5,5'-benzimidazole) (PBI) commercialized by Celanese Fibers Co. (Germany), has a very good thermal stability but, because of its meta-substitution and non-linear shape,

this polymer does not offer high strength and high modulus. The tensile properties of PBI fibers are in the range of conventional textile fibers [3,5]. As main applications of PBO it is possible to cite athletic equipment, high-fidelity speaker cones, heat and flame resistant work-wear such as for fire fighters and particular areas, such as the knee and elbow regions, of motorcycle suits are reinforced with PBO fabric, providing the required excellent heat, flame and abrasion resistance. PBI is mostly used in non-structural roles as high-temperature gas filtration, aircrafts fire blocking, nonwoven insulative products, among others [3,5,46].

Unlike the other two classes aromatic copolyesters are a thermotropic LCP (TLCP). These polymers possess a molecular structure with a high degree of linearity and rigidity allowing the formation of ordered phases on a wide temperature range. When these domains are extruded through very small holes, the flow and accompanying shear aligns the domains parallel to each other in the direction of flow. When cooled down, the extruded fiber has a highly oriented structure with high tensile strength and modulus. Because of this high orientation, drawing after spinning is not necessary, to improve the strength of a TLCPs increase the chain length is necessary. Solid-state polymerization of the spun fiber, which raises the molecular weight, results in fibers with very high strength and modulus [3,5,46]. The most known commercially available products of this class are Vectran® (Kuraray, Japan) a copolymer based on 4-hydroxybenzoic acid (HBA) and 6-hydroxy-2-naphthoic acid (HNA), Xydar® (Solvay Advanced Polymers, Belgium) and Ekonol® (Sumito Chemical, Japan) a copolymer of HBA, terephthalic acid  (TA) and 4,4'-biphenol (BP) [3]. Among the applications it is important to cite products including towed arrays/streamers for off-shore exploration, halyards for racing yachts, restraint lines for race cars, and long lines for tuna fishing. And the air bags used to land the Jet Propulsion Laboratory Pathfinder on Mars in 1997 were produced with TLCP fibrers because of the flex/fold characteristics (even at extreme low temperatures) and tear strength of composite fabrics made from the fiber [46].

### 2.2.3.1    Vectran®

A thermotropic aromatic copolyester fiber known as Vectran® was used in this work as matrix and reinforcement. Vectran® fibers are produced by spinning a LCP polymer developed under the trade name of Vectra®, which

is a copolymer of HBA/HNA with a molecular ratio of 73/23, respectively. Its molecular structure is showed in figure 6.
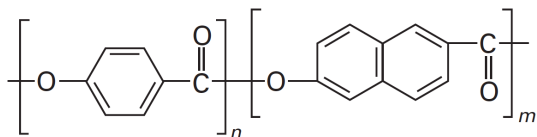
The main component of Vectran® is the HBA, this monomer is capable to form a whole aromatic chain conferring a rigid and linear molecular structure to the LCP. Nonetheless, it has a very high melting temperature (around 600 °C) and start to decompose before reaching this temperature, being impossible to melt-spin it. Due to this reason Hoechst-Celanese (USA) developed polymers based on parallel offset or 'crankshaft' geometry provided by 2,6 functionally di-substituted naphthalene monomers, in this particular case a HNA was used. The addition of HNA drop the Vectran® melting temperature to around 300 °C being possible to process it through conventional techniques. The copolymerization is one of the most effective techniques to decrease the crystallinity and melting temperature of a polymer, in particular with HBA/HNA copolymers the minimum melting temperature (245 °C) occurs at 40 mol% HNA [3,5,42,44].

Using X-ray diffraction techniques Blackwell et al [47] concluded that the sequence distribution of HBA/HNA copolymer is random. Windle [48] has suggested that this random sequence could be described as a non-periodic layer (NPL) crystal (figure 7(a)). In this model, the same random sequence in neighboring chains forms ordered, matching sequences by axial translations between adjacent chains. Alternatively, Blackwell and Biswas [49] have proposed a model suggesting the existence of random sequences as one-dimensional para-crystalline lattices (PCL) along the chain axis (figure 7(b)). The main difference between these two models is that the PCL model requires crystallites to form as close packing of random chains, without identical matching sequences between adjacent chains. Statistical interpretations have shown that the probability of finding matching monomer units decreases rapidly as one considers an increasing number of chains, favoring the PCL model. However, A modification of the PCL model

using ideas from the NPL model seems to give a more realistic physical image of the crystalline structures of the random liquid crystal copolyesters [50].
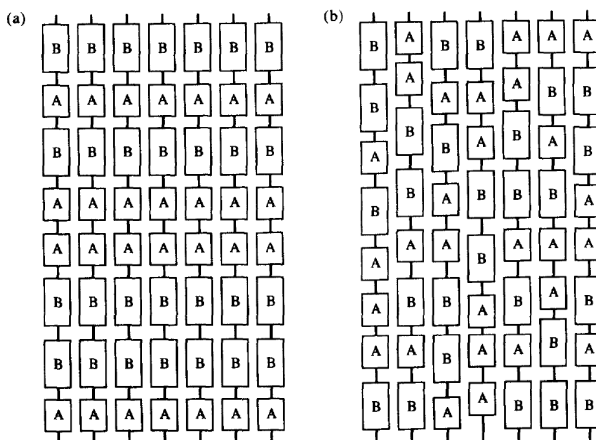
**Figure 7 -** Schematic two-dimensional representation of the order in the solid state of HBA/HNA copolymers as described by (a) the PCL model and (b) the NPL model [50].

There are two main paths to increase the thermal stability and the mechanical properties of the TLCPs, the first is the randomization process and the second is sequence ordering. Both are results of an annealing of the copolyesters near their crystallization temperature ($T_{CN}$). The first consists in the redistribution of monomer sequences in random copolymers and the variation of the materials microstructure after a transition from a solid crystal to a nematic melt. It was confirmed by Muhlebach et al. [51] that these processes are attributed to the inter-chain transesterification reactions. In polyesters, inter-chain transesterification reactions, would appear to have a number of useful implications as change of the polymer average molecular weight and molecular weight distribution, produce both blocky and random copolymer structures by blending high molecular weight polymers, and effectively perform localized post-processing steps in existing polymer structures [52].

On the other hand, the annealing of the copolyesters near the $T_{CN}$ increases their melting temperatures accompanied by a change in crystal structure (hexagonal to orthorhombic) and an increase in density. Annealing

HBA/HNA copolyesters near $T_{CN}$ dramatically increases the transition temperature throughout the entire compositional range. The melting transition of the annealed copolymer is best described as a smectic *B* (molecules arranged in a hexagonally close-packed array within the layers), and in addition there is an abrupt decrease in solubility.

Economy et al. [53] propose an ordering mechanism that is chemical in nature and depends on inter-chain transesterification reactions inside the existing crystallites present in the copolyester. Therefore, near $T_{CN}$ the end-groups have sufficient mobility within the crystallites to facilitate ordering of the microstructure through inter-chain transesterification reactions. These reactions can only occur in the crystallites, since in the coexisting nematic melt no templates are present to promote ordering. The driving force for chemical ordering reactions arises from the improved packing and correspondingly higher density associated with a more ordered structure. Inter-chain transesterification reactions allow an improved ordering of sequences, but not necessarily complete ordering, since mobility within the crystallites should drop significantly as the transition temperature begins to increase [52].

## *2.3    Electrospinning*

In order to produce polymeric fibers there are several traditional techniques extensively studied (e.g. melt spinning, solution spinning, dry spinning, gel spinning) however, these conventional techniques present as limitation the diameter of the produced fibers, that is generally in a range of 05 to 25 µm [22]. The diameter of these fibers can be further reduced, to a sub-micron level, submitting them to a drawing process [46,54]. In spite of this, electrospinning process appears as the most convenient and scalable technique for the nanofibers production. This process has been successfully scaled up and is used in the production of industrial products such as air filter media. Fibers with a diameter in the range 10 – 900 nm can readily be electrospun into mats [16,55].

The first observations of the electrospinning happened in the late 1500s where Gilbert described an electrostatic phenomena; a suitably charged piece of amber was brought near a droplet of water it would form a cone shape and small droplets would be ejected from the tip of the cone. Once again, in 1750, Nollet reported an electrostatic spraying of a liquid.

Although, the first description of an electrospinning process occurred in 1902 by Cooley when he applied a US patent number 692631, which describes a method of using high voltage power supplies to generate yarn. In 1934, Formhals [56] patented an improved version of the electrospinning process and apparatus. In his patent the fiber collector could be moved, allowing a certain degree of fibers orientation. Between 1964 and 1969 Taylor contributed to electrospinning by mathematically modeling the shape of the cone formed by the fluid droplet under the effect of an electric field, which is nowadays known as Taylor cone [55,57-59].

Nonetheless, until 1995 there are only a few number of publications regarding electrospinning [60]. Electrospinning was re-discovered in 1995 in the form of a potential source of nano-structured material by Reneker and Doshi who, while investigating electrospraying, observed that fibers could easily be formed with diameters on the nanometer scale [61].

The basic set-up for the electrospinning technique consists in three major components: a high-voltage power supply, a reservoir with a capillary tip for the spinning solution (or melt) and a collector (grounded conductor) an example can be seen in figure 8.
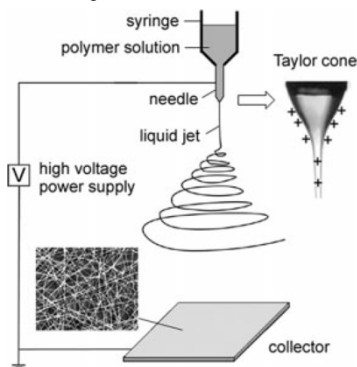


**Figure 8 –** Schematic representation of a basic electrospinning set-up [60].

The electrospinning consists in the application of a high electrical current to the needle and when the polymer solution (or melt) is pumped into it with a controlled rate, the pendant drop of solution in the needle tip will become highly electrified and will have the induced charges homogeneously distributed over the surface. The drop will experience two concurrent effects: the electrostatic repulsion between the surface charges and the Coulombic

force exerted by the external electrical field. These forces will deform the drop to a conical form, known as Taylor cone (figure 8). When the strength of electrical field exceeds a threshold value, the repulsive electrostatic force overcomes the surface tension and the charged jet is ejected from the tip of the Taylor cone. The jet starts a stretching and whipping process forming a long and thin thread, being continuously elongated reducing its diameter from hundreds of micrometers to tens of nanometers. Its small diameter permits rapid mass exchange and the solvent usually evaporates during its traveling from the capillary to the collector acting as a counter electrode. The result is a non-woven mat with nanofibers randomly oriented in it (figure 8). Under certain conditions the charged jet violates its continuity and, instead of fibers, nano- and/or microparticles of various forms are formed on the collector. This process is called electrospraying and is particularly appropriate for obtaining nano- and/or microparticles [12,16,59,60].

Reneker and Yarin [21,62] analyzed the jet as a system of connected, viscoelastic dumbbells and provided a good interpretation for the bending stability. Initially the jet only follows a direct path towards the counter electrode. Then it becomes unstable performing a series of bending coils with a continuously enlarged radius. Investigations with the help of a high-speed digital video camera show that the jet is only one and it moves and bends very quickly. From the above description it is clear that whipping instability is the primary mechanism responsible for reducing nanofiber dimensions during electrospinning. However, Dzenis [63] pointed out that suppressing this instability using either a secondary electric field or a short tip to collector distance did not result in substantially thick nanofibers being generated. Nowadays the understanding of the process is still incomplete, and all the factors that govern fiber formation are not well understood [55,58-60].

The morphology and diameter of the electrospun fibers are affected by several parameters that can be divided in three broad categories: solution parameters, processing parameters and environmental parameters.

The solution parameters include volatility of the solvent, dielectric constant, solution conductivity, surface tension, viscosity (concentration), and type of polymer. When a solvent with a very low volatility is used, wet fibers are collected on the other hand if the solvent is too volatile the Taylor cone will solidify, blocking the process. The dipole moment of the solvent and the solution conductivity must both be on a sufficient level to enable

electrospinning to occur, the fibers diameter will decrease with the increase of conductivity. If the surface tension is too high instability of jets will probably occur. In the case of concentration, if the solution present a low viscosity a mixture of fibers and beads will predominate, however if the viscosity is too high, the formation of fibers will be prohibited because of the inability to maintain the flow of the solution at the tip of the needle, resulting in the formation of larger fibers. Also, increasing the molecular weight of the polymer will reduce beads formation and a further increase of it will raise the fiber diameter [57,60,64].

Process parameters includes applied electric field, tip to collector distance, solution flow rate and type of collector. The applied voltage to the solution is crucial in the electrospinning; generally increasing its value causes greater stretching of the solution leading to a decrease in the fiber diameter and faster solvent evaporation. However, Zhang [65] and Demir [66] suggested that increasing the applied voltage causes more polymer ejection and consequently higher larger fiber diameters. There is a minimum and a maximum distance between tip and collector in which the electrospinning will produce fibers; outside this interval it will generate beads. Within this range it will be an optimal distance in which the evaporation of the fibers will be favored. The solution flow rate influences directly the jet velocity and the transfer rate. A lower flow rate lead more time to the solvent evaporate forming very thin and dry fibers, on the other hand higher flow rates form much thicker fibers and increase the incidence of beads. The collector geometry and the addition of secondary electrodes can be used to control deposition patterns or the extent of the bending instability. Works such as Teo and Ramakrishna [67] shows that the modification of the electric field allows control over the fiber flight and hence the modification of the final fiber alignment [57,60,64].

The environmental parameters are mainly temperature and humidity. Increasing the first causes a decrease of the fibers diameter; this is attributed to the decrease in the polymeric solution viscosity. Increasing the humidity during electrospinning generate the appearance of circular pores all over the fibers surface. High humidity can improve the discharging of the deposited electrospun fibers. In a dry ambient a volatile solvent evaporate fast, and in some cases it can evaporate inside the tip, solidifying the polymer and halting the electrospinning [57,60,64].

As demonstrated, electrospinning is a simple and powerful technique to generate nanofiber mats, there are a series of applications for the produced structures as main examples it is possible to cite: filtration (e.g. air filters, antimicrobial nanofilters, adsorptive membranes), biomedical field (e.g. enzyme immobilization, drug delivery, scaffolds in tissue engineering), clothing material, sensors, and as reinforcement in composite materials. Particularly in composite materials due to the nanofibers high surface-to-volume ratio, it use can improve the interaction between matrix and reinforcement leading to better mechanical properties. Beside the mechanical point of view, the addition of nanofiber mats can induce special functionalizations on the composite, in example self-healing capabilities [55,57,58,60,64,68].

## 2.4    *Predictive models*

The structure of composite materials with random orientation is highly complex; therefore, it is a great challenge to trace those structural parameters that affect the desired property. The simplest way to predict the elastic modulus is to use the rule of mixture and check if it fits. There have been many micromechanical theories and models developed to predict mechanical properties of fiber-reinforced composites, mostly of them focused on continuous and unidirectional composites. In example, the Voigt upper bound of the E-modulus is based on a two-phase laminate model (matrix and reinforcement), according to which the reinforcing laminates are aligned along the load direction and thus all constituents experience the same strain (parallel coupling), and the Reuss lower bound of stiffness reflects a serial coupling, according to which both matrix and reinforcing phases are under the same stress. On the other hand, a few micromechanical models have been established for discontinuous fiber composites.

Halpin and Tsai [69,70] developed a well-known composite theory for predicting the stiffness of unidirectional composites as a function of aspect ratio. This theory is based on the early micromechanical works of Hermans [71] and Hill [72]. Hermans generalized the form of Hill's self-consistent theory by considering a single fiber encased in a cylindrical shell of the matrix that is embedded in an infinite medium assumed to possess the average properties of the composite. Halpin and Tsai reduced Herman's

results into a simpler analytical form adapted for a variety of reinforcement geometries, including discontinuous filler reinforcement [73]. Halpin-Tsai equations are expressed in equations 1 and 2.

$$E_{LL} = E_m \frac{1 + \zeta_L \eta_L V_f}{1 - \eta_L V_f} \qquad (1)$$

$$E_{TT} = E_m \frac{1 + \zeta_T \eta_T V_f}{1 - \eta_T V_f} \qquad (2)$$

where $E_{LL}$ and $E_{TT}$ represent respectively the longitudinal and transverse tensile moduli for a unidirectional aligned fiber composite having the same fiber volume fraction and fiber aspect ratio of the composite under evaluation, $E_m$ is the matrix modulus, $V_f$ is the fiber volume fraction, and:

$$\zeta_L = 2\frac{l}{d} \qquad \zeta_T = 2 \qquad \eta_L = \frac{\frac{E_f}{E_m} - 1}{\frac{E_f}{E_m} + \zeta_L} \qquad \eta_T = \frac{\frac{E_f}{E_m} - 1}{\frac{E_f}{E_m} + \zeta_T}$$

being $l$ the length, $d$ the diameter and $E_f$ the tensile modulus of the fibers.

Based on the predictions of $E_{LL}$ and $E_{TT}$, several theories were proposed to estimate the in-plane elastic modulus of the random fiber composite ($E_R$); the first, and probably the more diffused, was proposed by Tsai and Pagano [74],

$$E_R = \frac{3}{8} E_{LL} + \frac{5}{8} E_{TT} \qquad (3)$$

a second one was proposed by Cox [75],

$$E_R = \frac{1}{3} E_{LL} \qquad (4)$$

and a third was proposed by Loewenstein [76],

$$E_R = \frac{3}{8} E_{LL} \qquad (5)$$

Lavengood and Goettler [77] used an approximate averaging technique to generate the following rule-of-thumb expression for the elastic modulus prediction of a structure having 3-dimensionally random fiber orientation;

$$E_R = \frac{1}{5} E_{LL} + \frac{4}{5} E_{TT} \qquad (6)$$

at 30 vol% loading, equation 6 predicts a value about 20% lower than the in-plane stiffness for random 2-dimensional orientation (equation 3) [78]. Nielsen [79] believes that the equation 6 predicts values which are too large for truly randomly oriented 3D composites when the concentration of fibers is below 40% [23].

Christensen [80] have used alternative approaches to arrive at upper and lower bounds for the stiffness problem. This approach can accommodate the general random 3-dimensional problem from a bounding viewpoint, but cannot explicitly accommodate the distributions of aspect ratio and fiber orientation [78].

The following model was proposed by Christensen and Waals [81] to predict the elastic modulus behavior on 3D randomly distributed short fiber composites for low fiber volume fractions ($V_f \leq 20\%$);

$$E_R = \frac{V_f}{6} E_f + [1 + (1 + \nu_m)V_f]E_m \qquad (7)$$

where $\nu_m$ is the Poisson's ratio of the matrix.

It was found that at low fiber volume fractions, the Christensen and Waals model predicted values higher than the experimental in a range of 0 - 15%, this difference was attributed to partially ineffective bonds and /or effects of the chopped fibers [82].

# Chapter III

## EXPERIMENTAL

### 3.1    Materials

Kuraray supplied the as-spun Vectran® LCP fiber yarn used in this work as matrix and reinforcement under the trade name of Vectran® NT. It has a linear density of 750 denier and 150 filaments per yarn and a sizing weaving finish applied at a level of ~ 0.5% oil-on-yarn to assist processing (e.g. rewinding, twisting, braiding, weaving). Vectran® is a copolymer of 4-hydroxybenzoic acid (HBA) and 2-hydroxy-6-naphthoic acid (HNA) with a molar ratio of 73/27, respectively [83,84]. Vectran® NT has molar mass of 290.27 Da and molecular weight higher than 20 kDa [85]. The fibers possess an almost circular cross-section with an average diameter of 25.5±2.1 μm.

Poly(ethylene oxide) (PEO, molar mass 44.05 Da, $M_w$ = 600 kDa, figure 9) was used as host polymer in order to increase the spinnability of Vectran® during the nanofibers production.
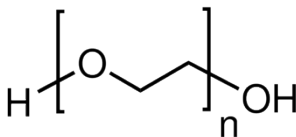


**Figure 9 –** Poly(ethylene oxide) molecular structure.

Chloroform (> 99.8%) and pentafluorophenol (PFP, > 98%) were used as solvents in the nanofibers production and were purchased from Sigma-Aldrich. All materials were used as received without any further purification.

The solid epoxy-resin with high molecular weight (D.E.R. - 669E), is a reaction product of a Bisphenol A-epichlorohydrin, having an epoxy equivalent weight between 3500 and 5500 was supplied by The DOW chemical company, to be used in this work as a coupling agent.

## 3.2 Composites preparation and characterization

### 3.2.1 Single Polymer Micro Composites (SPMCs)

#### 3.2.1.1 Sample preparation

The continuous Vectran® NT fibers have been chopped in 12 mm short fibers using a fiberglass chopper model B-410 (Glascraft Composites Equipment). The fibers were used in three ways; as received (for the matrix), after an annealing treatment (described in section 3.2.1.2) and annealed plasma treated (described in section 3.2.1.3), both as reinforcement.

In a first step the reinforcement and the matrix (as received fibers) were mechanically mixed at weight fractions of 10, 20 and 30%. The next step is the SPMCs consolidation; an aluminum square mold of 120 x 120 mm² and 1 mm thick was used. The mixture was placed between two 1 mm thick PTFE sheets and hot-pressed using a Carver laboratory press at a temperature between the melting points of the constituents (295 °C) once the consolidation temperature was reached the pressure was increased until 4.4 MPa and maintained for 30 seconds and then the SPMCs were cooled under pressure (1.8 MPa). In this way single polymer micro composite plates of LCP reinforcing fibers embedded in a LCP matrix were prepared. When used, an epoxy coupling agent it has been added in the composite as parts-per-hundred (phr) of matrix, maintaining the fiber/matrix ratio untouched, and it has been mechanically mixed together with the other components before the consolidation.

#### 3.2.1.2 Annealing treatment

In the past two decades annealing on liquid crystalline polymers was widely studied. Annealing treatments consist in increasing the fibers temperature close to the crystallization temperature ($T_{CN}$), and keeping them under these conditions for a pre-determined amount of time. The annealing used in the present work was motivated by the previous treatments successfully developed for commercial Vectran® microfibers [9-11,86,87].

The annealing treatment was optimized in order to increase the melting temperature and tensile properties of commercially available Vectran® NT fibers. The annealing was performed under vacuum in an oven

in the temperature range of 240 – 300 °C and treatment times lasting between 2 and 24 hours.

### 3.2.1.3    Plasma treatment

A plasma apparatus, consisting of a glass cylinder reactor (500 mm in length and 150 mm in diameter) equipped with semi cylindrical copper electrodes, was assembled at the University of Trento. A radiofrequency generator RF5S (maximum power 500 J.s$^{-1}$ and frequency 13.56 MHz) matching network AM-5 and controller AMNPS-2A supplied by RF Plasma Products, (Marlton, NJ, USA) were used. Vacuum, produced by a double stage pump, was controlled and measured by Edwards devices. The working pressure was ca. 1 atmosphere. The voltage of 30 V and a treatment time of 3 min were used in the fibers treatment; oxygen fluxed along the reactor axis at a flow rate of 100 ml/min.

### 3.2.1.4    Thermal analysis

Differential scanning calorimetry (DSC) measurements were performed using a Mettler DSC 30 Low Temperature Cell and a Mettler TC 15 TA Controller. The heating rate was 10 °C/min under a nitrogen flux of 100 mL/min.

Thermo-gravimetric analysis (TGA) was applied, and measurements were performed using a modulated TGA Q5000IR by TA instrument. The heating rate was 10 °C/min under an air flux of 25 mL/min.

### 3.2.1.5    Mechanical analysis

All tensile tests were conducted using a universal testing machine (Instron, model 4502). Tensile tests on the single fibers were executed according to ASTM standard D3379 with a 10 N load cell. Single fibers were randomly extracted from a bundle and mounted on window cards using quick-setting glue. The diameter of individual fibers was measured using an optical microscope. The gage length was fixed at 25 mm and the cross–head speed at 1 mm/min. At least 17 specimens were tested for each sample.

Tensile tests on composites were performed according to ISO 527 on 1BA specimens with a gage length of 25 mm, a crosshead speed of 1 mm/min and with a 1 kN load cell. The strain was recorded by using a

resistance extensometer Instron model 2620-601 with a gage length of 12.5 mm. At least five specimens were tested for each sample.

Dynamic mechanical thermal analysis (DMTA) under tensile configuration was performed by a DMA Q800 (TA Instruments, New Castle, USA) apparatus on rectangular specimens of 5 x 15 x 1 mm$^3$ at a frequency of 1 Hz. Storage modulus ($E'$) and loss tangent ($\tan \delta$) were determined in the temperature range from 0 °C up to 200 °C. A peak-to-peak displacement of 64 $\mu$m and a heating rate of 3 °C/min were imposed.

### 3.2.1.6    Infrared spectroscopy

Infrared analysis was performed in attenuated total reflection (ATR) mode using a Fourier transform infrared (FTIR) Spectrum One (Perkin Elmer). Each spectrum was generated as a mean of four scans between 4000 and 650 cm$^{-1}$. The spectral resolution was 4 cm$^{-1}$.

### 3.2.1.7    Observations

Field emission scanning electron microscopy (FESEM) images were obtained using a Supra 40 (Zeiss) microscope with the operating mode in high vacuum and secondary electron detector. Optical observations were done using a Leitz Ortholux 2 Pol microscope in transmission mode.

## 3.2.2    Single polymer nano composites (SPNCs)

### 3.2.2.1    Sample preparation

In a first step, two square plates of matrix (120 X 120 X 0.5 mm$^3$) were put in a hot-press at a temperature over their melting temperature (295 °C). After the homogenization of temperature and melting of the matrix plates the temperature was set down to a temperature bellow the melting temperature of the nanofiber mats (270 °C). Due to the solidification kinetics the matrix plates remains in the molten state, the nanofiber mats were positioned over one matrix plate and the other matrix plate was positioned in the top of then forming a sandwich composite. The next step is the SPNCs consolidation itself; inside an aluminum square mold (120 X 120 X 1 mm$^3$) the composite was hot-pressed using a Carver laboratory press at a temperature slightly

bellow the melting point of the nanofiber mats and the pressure was increased until 4.4 MPa during 30 seconds and then the SPNCs were cooled under pressure (1.8 MPa). In this way single-polymer composites of Vectran® nanofibers embedded in a LCP matrix were prepared.

### 3.2.2.2    Vectran® nanofibers preparation

Vectran® solution (1 wt%) was prepared by dissolving 0.202 g of LCP in 20 g of a mixture of two solvents, chloroform and pentafluorophenol (PFP), with a 70/30 ratio by weight, respectively. Stirring for 10 h at room temperature resulted in a yellow-clear solution. PEO solution (1.85 wt%) was prepared by dissolving 0.37 g of PEO in 19.63 g of chloroform under magnetic stirring for 5 h. Then, the Vectran® solution was mixed with the PEO solution at a ratio of 15:1 by weight, respectively. The as-spun nanofibers produced in the present work possess the Vectran®/PEO weight ratio of 8.19:1, correspondingly.

To spin Vectran® or its blends with PEO, a conventional electrospinning setup was used (figure 8), with aluminum foil as a collector [62]. The controlled power generator was a Glassman High Voltage model EH, that can generate DC voltage in the range 0 – 30 kV. A pump NE-1000 from New Era Pump Systems, Inc. was used to ensure a continuous supply of polymer solution during the process. The voltage was set at 10 kV at a solution flow rate of 1.5 ml/h, and the distance between the collector and needle was kept equal to 10 cm. The obtained samples were dried for 24 h at room temperature.

### 3.2.2.3    Heat treatment

The heat treatment over the nanofiber mats was used to enhance the mechanical properties of Vectran®, as well as its melting temperature and remove the residual PEO used as "host" polymer during the electrospinning. The heat treatment was performed in an oven in air in the temperature range 250 – 300 °C, and the treatment duration were in the range 15 – 24 h.

### 3.2.2.4    Thermal analysis

Differential scanning calorimetry (DSC) measurements were performed using a Mettler DSC 30 Low Temperature Cell and a Mettler TC 15 TA

Controller. The heating rate was 10 °C/min under a nitrogen flux of 100 mL/min.

Thermo-gravimetric analysis (TGA) measurements were performed using a modulated TGA Q5000IR by TA Instruments. The heating rate was 10 °C/min under a nitrogen flux of 25 mL/min.

### 3.2.2.5    Mechanical analysis

Electrospun nanofiber mats were cut into rectangular specimens measuring 4 X 30 mm$^2$ and mounted on window-like holders with a gage length of 20 mm. Tensile tests were conducted with 15 as-spun mat specimens. Also a sample (consisting of 13 heat-treated specimens) was subjected to tensile test. The tensile tests were conducted using a universal testing machine (Instron, model 4502) with a 10 N load cell (Instron, model 2518-808) at a cross-head speed of 5 mm/min.

Tensile tests on composites were performed according to ISO 527 on 1BA specimens with a gage length of 25 mm, a crosshead speed of 1 mm/min and a 1 kN load cell. The strain was recorded by using a resistance extensometer Instron model 2620-601 with a gage length of 12.5 mm.

### 3.2.2.6    Microscopic observations

Field emission scanning electron microscopy (FESEM) images were obtained using a JEOL JSM-6320F and Supra 40 Zeiss microscopes under high vacuum and secondary electron detector operating mode. Transmission electron microscopy (TEM) was performed using a JEOL JEM-3010 microscope. Optical observations were done using an Olympus BX51 microscope in refraction mode and a Leitz Ortholux 2 Pol microscope in transmission mode.

### 3.2.2.7    Selected area electron diffraction (SAED)

Selected area electron diffraction (SAED) method is similar to X-ray diffraction but uses electrons rather than X-rays. Because of that, the examined region can be as small as a few nanometers. SAED images are obtained by using an aperture in the virtual image plane of the microscope to select a region of interest such as an individual nanofiber. Only the electrons falling inside the dimensions of the aperture will be analyzed. The

resulting scattered electrons are then imaged in the diffraction mode of the microscope. The circular pattern that appears is in essence a two-dimensional scattering pattern. This two-dimensional nature gives extra information about the orientation of the lattice scattering planes compared to a one-dimensional X-ray diffraction pattern[88].

# Chapter IV

## RESULTS AND DISCUSSION

### *4.1     Single polymer micro composites (SPMCs)*

In order to successfully produce SPMCs the first step is to obtain a difference in terms of melting temperature and mechanical properties between matrix and reinforcement. At this aim, a thermal annealing treatment has been optimized. In a second step, SPMCs have been produced by a thermal consolidation process and their thermo-mechanical properties have been investigated.

### 4.1.1     Annealing treatment on Vectran® NT fibers

The annealing treatment used in the present work was motivated by the previous treatments successfully developed for commercial Vectran® fibers [9-11,87]. Economy et al. [53] reported that after an annealing at temperatures higher than the crystal-to-nematic transition ($T_{CN}$) a chemical randomization occurs through transesterification. Depending on the annealing conditions, an endotherm peak may appear at temperatures lower than the annealing temperature. To understand the influence of the annealing temperature, DSC analysis on fibers treated at 240 °C, 260 °C, 280 °C and 300 °C for 2 hours were performed. As it can be observed in figure 10(a), the thermograms of untreated fibers present two wide endothermic peaks ($Tp_1$ and $Tp_2$), probably related to an orthorhombic to nematic transition [9,83,89]. After the thermal annealing treatment, a new

endothermic peak ($Tm_1$) appears at a temperature that increases with the annealing temperature. As reported in previous studies $Tm_1$ could be attributed to inter-chain transesterification reactions where an increase of alternating copolymer sequences occurs [53,83,89], or it can be associated to a process called crystallization induced reactions (CIR). In this process the initial non-crystalline random copolyester is converted to a block copolymer via ester interchange reactions in the solid state, replacing in this way the non-crystallizable unit sequence by crystallizable regions increasing the crystal size, crystallinity and melting point [11,53]. When the treatment was performed at 300 °C, $Tm_1$ overlaps the endothermic peaks $Tp_1$ and $Tp_2$ present in the untreated fibers becoming the new transition temperature of the fibers. Due to the larger increment in $Tm_1$ temperature, 300 °C was chosen as annealing treatment temperature. In order to establish an optimal treatment time, DSC analysis were also performed on fibers treated at 300 °C for 2, 6, 9, 12, 15, 19 and 24 hours. The DSC traces of Vectran® fibers as a function of treatment time at 300 °C are presented in figure 10(b). It is interesting to observe that until 15 hours of treatment $Tm_1$ moves to higher temperatures with increasing treatment times. After this time, $Tm_1$ starts to decrease, probably due to concurrent degradative phenomena. The annealing at 300 °C for 15 hours in inert atmosphere effectively increased the melting point of Vectran® NT fibers by almost 30 °C. Therefore, this conditions were selected for an optimal treatment. For comparison purposes, on both figure 10(a) and 10(b) the thermogram of commercially available Vectran® HS fibers is reported. Vectran® HS fibers are commercially available and have been subjected to a proprietary heat treatment under tension [90].
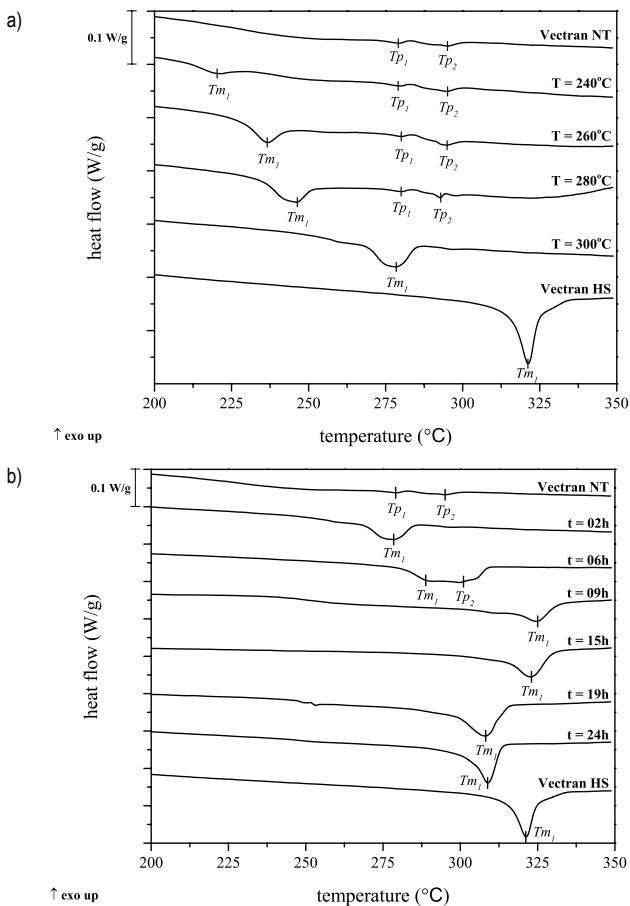
**Figure 10 –** DSC traces on Vectran® fibers as a function of a) annealing temperature for 2 hours and b) annealing duration at 300 °C.

The increase of the melting temperature of the fibers was not the only aim of the annealing treatment, figure 11 shows the representative tensile curves of Vectran® NT, annealed at 300 °C for 2 hours, annealed at 300 °C for 15 hours ad Vectran® HS. After only 2 hours of annealing there are no considerable modifications in the mechanical properties of the material in comparison with the as-received fibers. It is worthwhile to observe that after 15 hours of annealing at 300 °C, the fibers increase their tensile strength by 35% and elongation at break by 12% in comparison with pristine Vectran®

33

NT fibers. However, the tensile modulus of all kinds of fibers does not change significantly. The improvement on the tensile properties of LCP fibers has been attributed to the increase in molecular weight after the treatment due to the transesterification reactions induced by the thermal annealing [9,11]. Vectran® HS fibers present nearly the same elastic modulus but a much higher tensile strength and elongation at break due to the proprietary heat treatment under tension they have been submitted to. It is important to underline that, due to the impossibility of using an extensometer directly on the fibers, all the elastic modulus were corrected by taking the machine compliance into account.
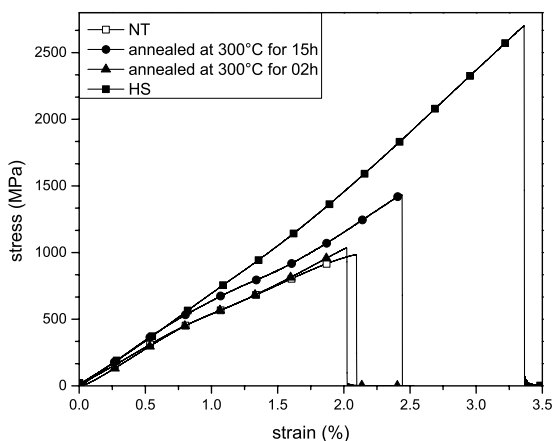


**Figure 11 –** Example of tensile stress-strain curves of Vectran® single fibers.

Materials break in correspondence of their weakest points or from regions of stress concentration. Testing a fiber in tension involves applying a load to it and determining the load at which it breaks. If such a tensile test is conducted on many specimens, usually a large scatter in breaking loads is observed within the population tested [3]. This behavior can be treated using the classical (two-parameter) Weibull distribution. In particular, the cumulative distribution function $F(\sigma)$, which represents the failure probability for an applied stress $\sigma$, assumes the following expression [91,92]:

$$F(\sigma) = 1 - exp\left[-\left(\frac{\sigma}{a}\right)^b\right] \qquad (8)$$

where $a$ and $b$ are the scale and shape parameters, respectively. The shape parameter describes the dispersion of the strength values and it increases as the dispersion of the strength values decreases. The scale parameter is proportional to the average fiber strength.

Figure 12 report the cumulative probability of failure of pristine Vectran® fibers and after annealing. After a 2 hour annealing the shape parameter slightly changed in comparison with the pristine NT fiber. After 15 hours of annealing treatment the shape parameter value increased moving in the direction of HS fibers, i.e. of commercially available thermally treated fibers.
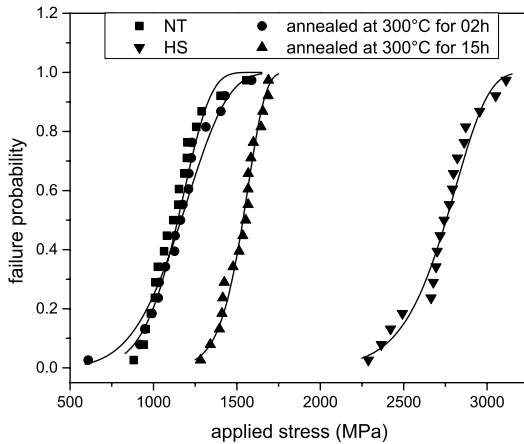


**Figure 12 –** Cumulative probability of failure for Vectran® NT, Vectran® HS and annealed fibers.

The found shape parameters of 8.16 for Vectran® NT, 15.02 for Vectran HS, 5.88 for 2 hour annealed and 15.60 for 15 hour annealed fibers, are higher than those commonly reported for E-glass (2–5) and carbon fibers (4–6). Those of NT and 2 h annealed fibers are lower than those of aramid fibers (8–14) and those of HS and 15 h annealed fibers are in the same range. Weibull scale parameters of 1198 MPa for Vectran® NT, 2823

MPa for Vectran® HS, 1240 MPa for 2 hour annealed and 1573 MPa for 15 hour annealed fibers, at a reference length of 25 mm were found. These values are comparable to the ones found in literature [6,7]. Table 1 compares the main tensile mechanical properties of as-received and annealed single fibers.

**Table 1 –** Results of single fiber tensile tests on untreated or annealed Vectran® NT fibers.

| Property | Vectran® NT | annealed at 300 °C for 02 h | annealed at 300 °C for 15 h | Vectran® HS |
|---|---|---|---|---|
| Tensile modulus [GPa] | 61.6 ± 3.2 | 54.3 ± 10 | 61.4 ± 8.8 | 66.8 ± 8.5 |
| Tensile strength [MPa] | 1129.6 ± 168.0 | 1148.0 ± 214.8 | 1521.6 ± 117.2 | 2726.7 ± 216.9 |
| Elongation at break [%] | 2.09 ± 0.24 | 2.00 ± 0.22 | 2.33 ± 0.24 | 3.75 ± 0.51 |
| Weibull scale parameter (MPa) | 1198 | 1240 | 1573 | 2823 |
| Weibull shape parameter | 8.16 | 5.88 | 15.60 | 15.02 |

Once the effectiveness of the annealing over the thermal and mechanical properties was attested, infrared spectroscopy was used to ensure that no chemical reactions occur during the treatment. In figure 13 it is possible to note that the peaks of aryl-ester absorbance (1739 cm^{-1}), aromatic C–C stretching (1610 cm^{-1}) and O–C–C stretching (1178 cm^{-1}) [11,93] remains unchanged after the annealing treatment in comparison with the pristine and Vectran® HS fibers. This is a strong indication of absence of chemical modifications during the annealing process, thus confirming that an increase of alternating copolymer sequences occurs, which is responsible of an increase of the melting temperature and of the mechanical properties of the annealed fibers.
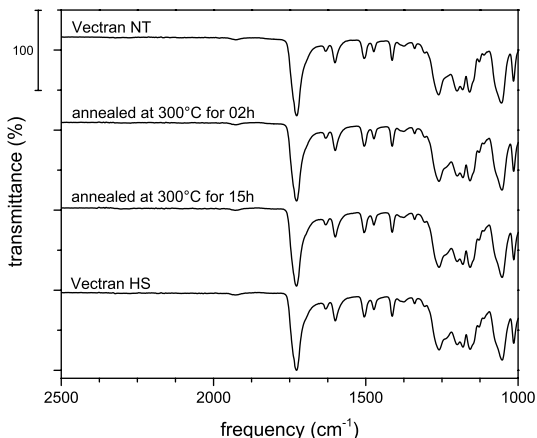
**Figure 13 –** FTIR spectra of Vectran® fibers before and after annealing.

Once the annealing treatment (300 °C for 15 h) was optimized over the reinforcement the SPMCs were produced.

### 4.1.2 Optimization of processing conditions and compatibilization for SPMCs preparation.

To optimize the consolidation temperature of SPMCs, a preliminary investigation has been conducted producing plates of unfilled matrix (Vectran® NT). They were produced at four different temperatures 265 °C, 275 °C, 285 °C and 295 °C. At 265 °C only a partial melting occurred generating a non-homogeneous plate that was not submitted to further evaluations. In table 2 tensile properties of the consolidated plates at different temperatures can be found.
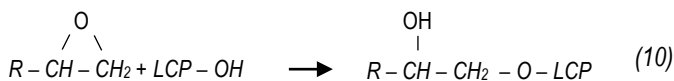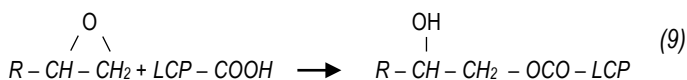
**Table 2 -** Tensile properties of unfilled matrix at various consolidation temperatures.

| Property | 275 °C | 285 °C | 295 °C |
|---|---|---|---|
| Tensile modulus [GPa] | 1.14 ± 0.24 | 1.22 ± 0.32 | 1.31 ± 0.14 |
| Tensile strength [MPa] | 31.4 ± 13.5 | 33.5 ± 14.6 | 37.7 ± 9.2 |
| Elongation at break [%] | 4.62 ± 1.41 | 4.75 ± 1.53 | 5.00 ± 1.44 |

The plate consolidated at 295 °C shows better mechanical properties as well smaller standard deviations in it results, therefore this temperature was chosen for the consolidation process.

In order to improve the interfacial fiber-matrix adhesion, surface modifications of the reinforcing fibers and the use of coupling agents are commonly used, on LCPs in particular, previous works using both techniques reported very good improvements in the interfacial adhesion [85,94,95]. In this work both techniques were studied distinctly, the use of a high molecular weight epoxy resin (D.E.R. – 669E) as coupling agent and the use of a plasma treatment over the reinforcement fibers as surface modification treatment.

The use of coupling agents for LCPs was widely studied and the reactive compatibilization seems to be the most promising technique. It combines the matrix and reinforcement through a suitable multifunctional coupling agent and the *in-situ*-formed copolymers, made of chain segments identical to the base constituents, should be effective compatibilizers of the composite. Epoxy resins of various epoxy equivalent weight (EEW) have been demonstrated to be excellent in compatibilizing blends whose single constituents possess functional groups able to react with the epoxy functions under melt conditions to form block copolymers of the blend pairs [95-98]. The D.E.R. – 669E it is not miscible to the LCP [97]. The only expected reactions are between the epoxy groups with the carboxylic acid or hydroxyl end groups of the LCP. They are demonstrated in the following reaction schemes (9) and (10) [98,99].

$$R - \overset{\displaystyle \overset{O}{\diagup \diagdown}}{CH - CH_2} + LCP - COOH \longrightarrow R - \overset{\displaystyle \overset{OH}{|}}{CH - CH_2} - OCO - LCP \qquad (9)$$

$$R - \overset{\displaystyle \overset{O}{\diagup \diagdown}}{CH - CH_2} + LCP - OH \longrightarrow R - \overset{\displaystyle \overset{OH}{|}}{CH - CH_2} - O - LCP \qquad (10)$$

In order to ensure that the D.E.R. – 669E will not suffer from any degradative phenomena during the composite consolidation due to the elevated temperature (295 °C), TGA analysis was made under air atmosphere, to mimic the consolidation atmosphere. It curve can be seen in figure 14, it is possible to note that the degradation onset is around 390 °C,

attesting in this way that the D.E.R. – 669E resin can be used as coupling agent, without suffering any degradation.
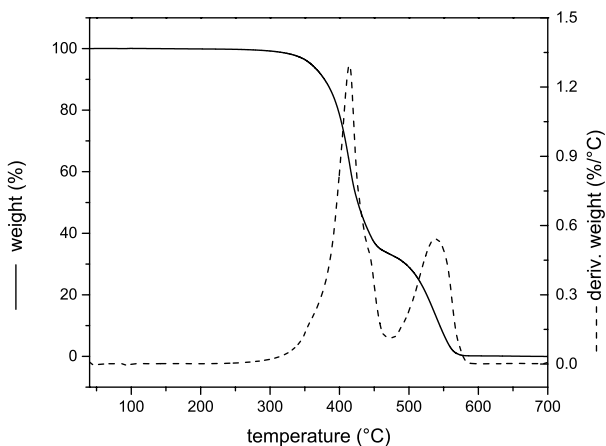


**Figure 14 –** Thermogravimetric curve of D.E.R. – 669E.

The plasma treatment was used in order to activate the surface of the annealed Vectran® fibers, in other words to clean their surface and introduce some chemical groups onto the polymeric chain. The microetching is the removal by evaporating surface material for cleaning purposes, in it the plasma breaks the carbon-to-carbon bonds of the hydrocarbon polymer, their volatile monomers and oligomers boil off and are removed away with the vacuum. This cleaning procedure removes external organic contaminants (such as hydraulic oils and sizings applied during the production) from the polymer surface. After the initial cleaning stage, the fibers surface is exposed to the plasma environment, the electrons, ions and free radicals in the plasma act on the surface, creating free radicals in the molecular chains of the polymer surface [100-103].

Oxygen plasma is very effective at increasing the surface energy, which translates to better wetting and greater chemical reactivity of the modified surface improving its adhesion and permanency [100,101].

### 4.1.3  SPMCs characterization

#### *4.1.3.1  Microstructure*

FESEM micrographs of the fracture surfaces of SPMCs filled with 20 wt% of annealed fibers, plasma treated annealed fibers and composites using D.E.R. – 669E as coupling agent are reported in figure 15(a – e).

First of all, it is important to note that, due to the proper thermal annealing, the fibers are able to maintain their structure and appear to be homogenously surrounded by a polymeric matrix generated by the melting of the as received Vectran® NT fibers. This confirms the suitability of the selected processing conditions to generate a single polymer micro composite based on short fiber of liquid crystalline polymer. It is also interesting to observe that, figures 15(a) and 15(b) shows the presence of distributed pull-out phenomena instead of fiber breakage, thus indicating the existence of a poor fiber-matrix interface. On the other hand, the fracture surface of SPMC filled with 20 wt% plasma treated annealed fibers (figure 15(c)) revealed mostly fiber breakage phenomena attesting the improvement in terms of interfacial adhesion between matrix and reinforcement. In figure 15(d) it is possible to note that in the composite filled with 20 wt% of annealed fibers and 0.5 phr of D.E.R. – 669E there is a diffused presence of pull-out phenomena as it happens in the SPMCs without the coupling agent, there are also traces of the epoxy resin in the fracture surface. The SPMCs containing 20 wt% annealed fibers and 2.0 phr of D.E.R. – 669E displays the same diffuse pull-out phenomena and in addition to that an agglomeration of the coupling agent in the fracture surface, as showed in figure 15(e), it is possible to conclude that increasing the amount of D.E.R. – 669E in the composite, over 0.5 phr, the epoxy resin tend to form aggregates that can act as defects causing a premature failure of the composite.
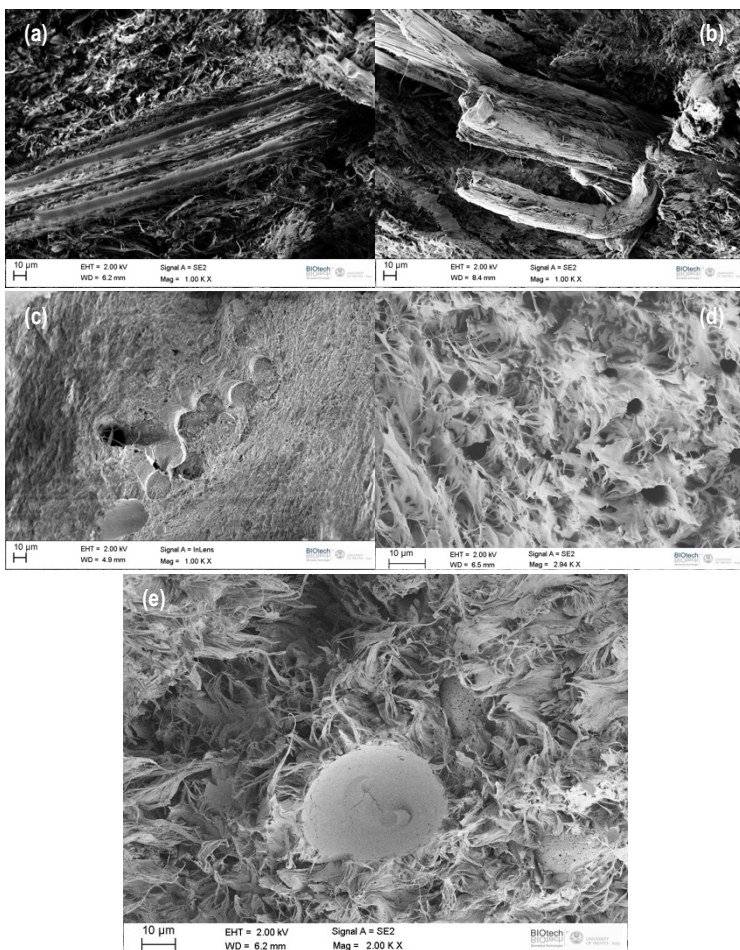
**Figure 15 –** FESEM micrographs of fracture surfaces of SPMCs filled with 20 wt% of annealed fibers [a) and b)], and c) plasma treated annealed fibers d) annealed fibers and 0.5 phr of D.E.R. – 669E e) annealed fibers and 2.0 phr of D.E.R. – 669E.

### 4.1.3.2    Thermal analysis

DSC technique on the SPMCs can give us important indications about their thermal behavior. The first information is to ensure that the reinforcement was not melted down during the SPMCs' consolidation and it is still as reinforcement, improving its mechanical properties. After a second

scanning, it is possible to have an indication of their recyclability from a thermal point of view.

As the DSC first scans (figure 16) shows in all the compositions, with the exception of unfilled matrix, is possible to observe two endothermic peaks. The first peak occurs around 282 °C and is present also on the unfilled matrix, it corresponds to the melting temperature of the matrix after the consolidation process. The second peak occurs between 295 and 305 °C and is present in all reinforced SPMCs, it is related to the melting temperature of the annealed fibers that reinforces the SPMCs. The presence of the peak confirms the presence of the reinforcement fibers after the consolidation.
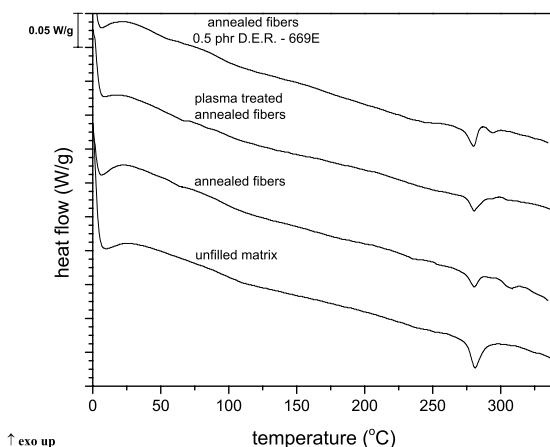


**Figure 16 –** First scan DSC curves comparing SPMCs containing different types of reinforcement and the unfilled matrix.

Figure 17 shows the DSC curves of the second scan, which means that the material was entirely melted down before this scan. Unlike the first scan, the second scan show only one endothermic peak for all the analyzed SPMCs, the peak occurs around 282 °C for all the compositions similar to the unfilled matrix. This indicates that the materials are fully recyclable, on a thermo analytical point of view, confirming one of the main ideas of the SPCs concept.
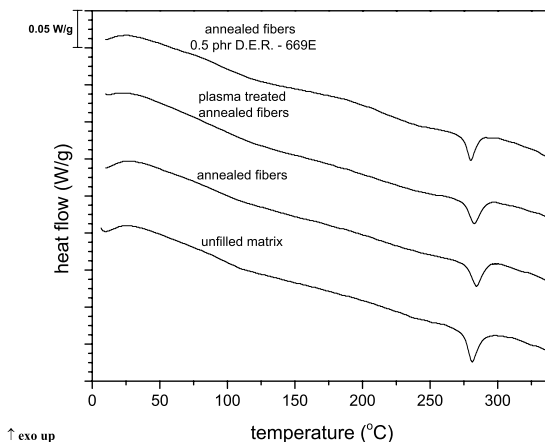
**Figure 17 –** Second scan DSC curves comparing SPMCs containing different types of reinforcement and the unfilled matrix.

### 4.1.3.3 Infrared spectroscopy

Another way to confirm the fully recyclability of the SPMCs produced in this work is to analyze their FTIR spectra after they had been melted down to see if there are changes in their chemical structure. Figure 18 shows the IR spectra obtained after the melting of the SPMCs and the unfilled matrix, it is important to note that in all cases the peaks of aryl-ester absorbance (1739 $cm^{-1}$), aromatic C–C stretching (1610 $cm^{-1}$) and O–C–C stretching (1178 $cm^{-1}$) [11,93] remains unchanged after the consolidation process and re-melting of the composite. The only changes in the chemical structure of the SPMC occur with the addition of the coupling agent. Due to its reactive compatibilization, two new peaks are formed at around 2925 $cm^{-1}$ and 2855 $cm^{-1}$ which can be attributed to the C–H stretching induced by the *in-situ* reactions due to the addition of the D.E.R. – 669E.

43
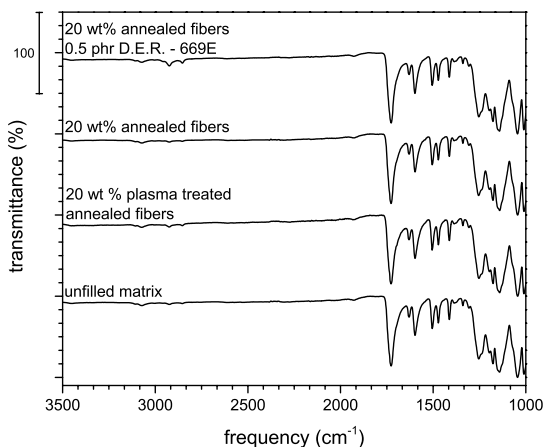
**Figure 18 –** FTIR spectra comparing SPMCs containing different types of reinforcement and the unfilled matrix after being melted down.

### 4.1.3.4    *Dynamic   mechanical   thermal   analysis (DMTA)*

In Figure 19(a) the storage modulus ($E'$) as a function of temperature is reported for neat matrix, SPMCs containing various amounts (10, 20, 30 wt%) of annealed fibers and 20 wt% of plasma treated annealed fibers. As the amount of reinforcement increases also the value of the storage modulus improves. The composite containing plasma treated annealed fibers presents a higher increment in the storage modulus in comparison with the sample containing the same amount of fibers without a surface treatment. This behavior is certainly due to a higher interfacial adhesion between matrix and reinforcement. The $tan\delta$ curves are reported in Figure 19(b) for the same systems. It can be easily noted that $tan\delta$ curves do not change substantially with the presence of annealed Vectran® fibers, even when they are plasma treated.

44
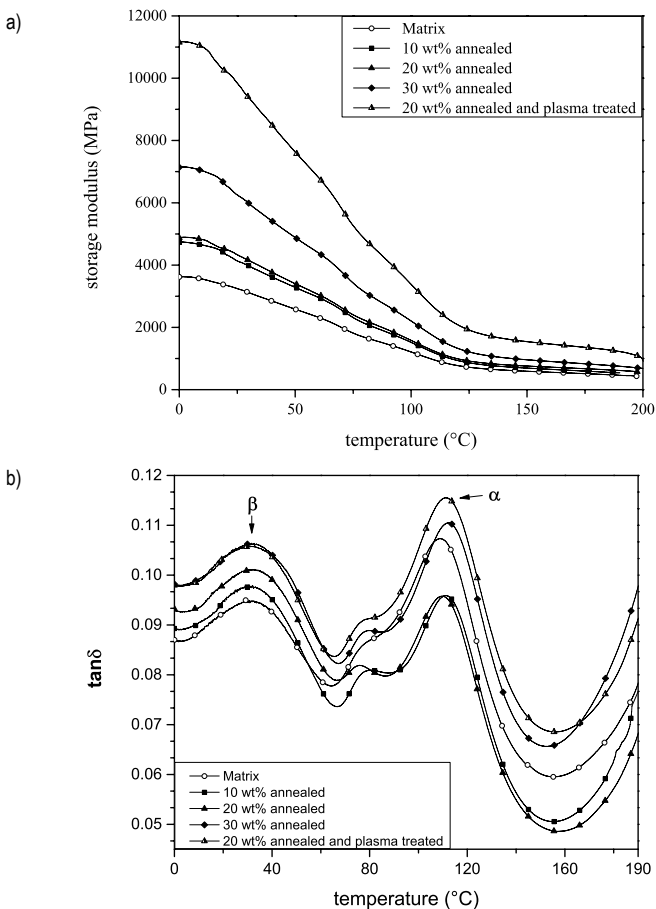
**Figure 19 –** DMTA curves on SPMCs as a function of temperature: a) storage modulus ($E'$), b) loss tangent ($tan\delta$).

In figure 19(b) it is possible to identify two thermal transitions that are generally named $\alpha$ and $\beta$. The first one represents the relaxation of the overall chain and corresponds to the beginning of the nematics phase mobility. The second one is attributed to the motions inside of the HNA group (C–O bond rotation) [11,104]. The $\beta$ transition does not change its temperature with the addition of the reinforcement, on the other hand, its intensity increase with the increasing of fiber content. The $\alpha$ transition temperature slightly increases with the addition of the annealed fibers.

On the figure 20 the $tan\delta$ curves of the composites containing several phr of coupling agent and the composites containing 20 wt% of annealed fibers are reported. It is interesting to note that unlike the use of surface treatments the use of epoxy resin as coupling agent causes modifications in the composites microstructure, this can be attested due to a higher temperature and wider $\beta$ transition and also the reduction in the temperature of the $\alpha$ transition with the increase of coupling agents amount in the composite.
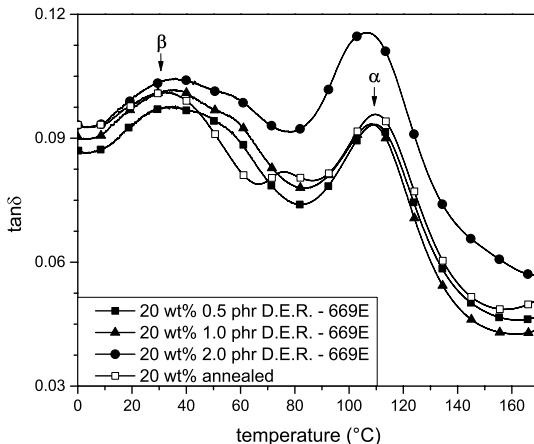
**Figure 20 -** Loss factor ($tan\delta$) as a function of temperature for SPMCs containing diferent amounts of coupling agent.

### 4.1.3.5    Mechanical properties

The first observation about the tensile tests on the produced composites is that the addition of the reinforcement does not change the failure mode (brittle behavior) in comparison with the unfilled matrix. Table 3 compares the tensile properties of the unfilled matrix with the SPMCs produced containing different weight fractions of reinforcement and in figure 14 examples of stress-strain curves are drawn. The evaluation of the reinforcement effect can be made with the help of the stress-strain curves and their tensile properties.

It is worthwhile to note that composites with 10 wt% of reinforcement do not manifest a significantly improvement of the tensile properties. On the other hand, when the reinforcement is raised to 20 wt% the tensile modulus

increases by 35% and with a further increment in the reinforcement content (up to 30 wt%) a noticeable increment of 161% in the tensile modulus can be observed. At the same time, all the investigated SPMCs manifest an expected decrease in the elongation at break with respect to the unfilled matrix. Varying the amount of reinforcement used does not significantly influence the tensile strength of the produced SPMCs.

**Table 3 –** Tensile properties of unfilled matrix and SPMCs at different weight fractions of annealed Vectran® NT fibers.

| Property | unfilled matrix | SPMC (10 wt%) | SPMC (20 wt%) | SPMC (30 wt%) |
|---|---|---|---|---|
| Tensile modulus [GPa] | 1.31 ± 0.14 | 1.30 ± 0.12 | 1.77 ± 0.10 | 3.42 ± 0.67 |
| Tensile strength [MPa] | 37.7 ± 9.2 | 33.8 ± 5.6 | 33.2 ± 4.6 | 29.3 ± 4.0 |
| Elongation at break [%] | 5.00 ± 1.44 | 3.71 ± 0.77 | 2.59 ± 0.56 | 0.79 ± 0.20 |
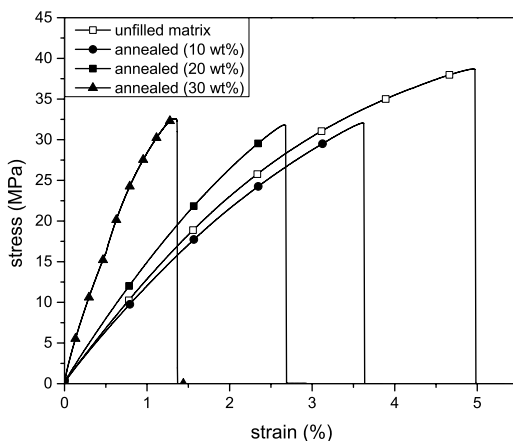


**Figure 21 –** Representative stress-strain curves of unfilled matrix and SPMCs containing 10, 20 and 30 wt% of annealed fibers.

According to FESEM observations (section 4.1.3.1), a poor interfacial adhesion was evidenced when annealed fibers where used. This behavior could be tentatively explained by considering the presence of a finishing on the Vectran® NT fibers. The finishing is added to the fibers during their
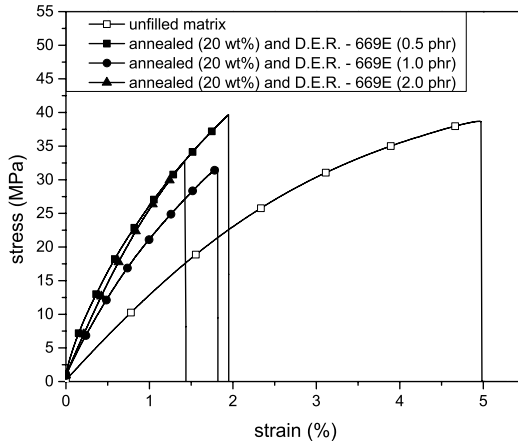
47

production, with the aim to compact the yarns, avoiding the adhesion between them, and favoring the typical processes adopted for traditional composite manufacturing. Once we are producing a SPC, the presence of such sizing may be the cause of a lack in terms of interfacial adhesion between matrix and reinforcement; also chemical changes could occur in the sizing during the annealing treatment developed in this work, hindering a good fiber-matrix interface.

Table 4 shows the results of the SPMCs containing different amounts of coupling agent (0.5, 1.0 and 2.0 phr) and reinforced with annealed Vectran® fibers (20 wt%). In figure 22 an example of their stress-strain curves is drawn. After the addition of only 0.5 phr of coupling agent it is possible to note a large increase in the elastic modulus (55%) as well as some increase on the tensile strength (11%) and an expected decrease of elongation at break in comparison with the composite without the coupling agent. This increase of the mechanical properties of the composite could be related with the homogeneous presence of the epoxy resin in the fracture (figure 15(d)). By increasing the amount of coupling agent it is possible to note a decrease of the tensile strength, as well of the tensile modulus and the elongation at break. This behavior can be explained by an agglomeration of the epoxy resin, since the latter is not miscible to LCP, generating defects instead of acting as a coupling agent causing, in this way, a premature failure of the composite. FESEM micrographs (section 4.1.3.1), had confirmed this behavior.

**Table 4 –** Tensile properties of SPMCs with and without coupling agents at 20 wt% of annealed Vectran® NT fibers.

| Property | SPMC (20 wt%) | SPMC D.E.R. - 669E (0.5 phr) | SPMC D.E.R. - 669E (1.0 phr) | SPMC D.E.R. - 669E (2.0 phr) |
|---|---|---|---|---|
| Tensile modulus [GPa] | 1.77 ± 0.10 | 2.74 ± 0.57 | 2.42 ± 0.26 | 2.51 ± 0.24 |
| Tensile strength [MPa] | 33.2 ± 4.6 | 37.0 ± 7.2 | 32.9 ± 6.6 | 29.3 ± 6.4 |
| Elongation at break [%] | 2.59 ± 0.56 | 1.92 ± 0.54 | 1.96 ± 0.42 | 1.54 ± 0.45 |

**Figure 22 –** Representative stress-strain curves of unfilled matrix and SPMCs containing 20 wt% of annealed fibers and various amounts of D.E.R – 669E (0.5, 1.0 and 2.0 phr).

The results of the tensile properties on SPMC containing 20 wt% of annealed and plasma treated annealed fibers are summarized in table 5, also representative stress-strain curves can be seen in figure 23. A remarkable improvement of 178% in the tensile modulus with respect to the unfilled matrix can be observed. On the other hand, in terms of tensile strength the composite with plasma-treated fibers maintained the same behavior of the composite with fibers without the plasma treatment. As a predictable result, the elongation at break shows a further decrease in its value since this property is directly related to the fiber-matrix interface, thus attesting the efficacy of the plasma treatment. FESEM observations, confirmed the better fiber/matrix compatibility when plasma treated annealed fibers are used as reinforcement.

**Table 5 –** Tensile properties of unfilled matrix, and SPMC with 20 wt% of annealed fibers and annealed fibers with a plasma surface treatment.

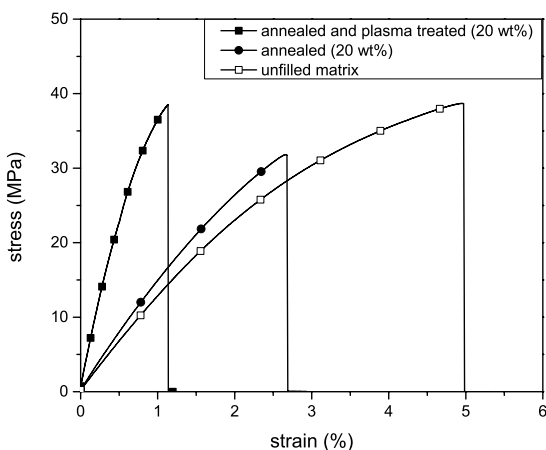| Property | unfilled matrix | SPMC annealed fibers (20 wt%) | SPMC plasma treated annealed fibers (20 wt%) |
|---|---|---|---|
| Tensile modulus | 1.31 | 1.77 | 3.64 |
| [GPa] | ± 0.14 | ± 0.10 | ± 1.30 |
| Tensile strength | 37.7 | 33.2 | 31.7 |
| [MPa] | ± 9.2 | ± 4.6 | ± 11.0 |
| Elongation at | 5.00 | 2.59 | 0.73 |
| break [%] | ± 1.44 | ± 0.56 | ± 0.16 |



**Figure 23 –** Representative stress-strain curves of unfilled matrix and SPMCs containing 20 wt% of annealed fibers and 20 wt% of plasma treated annealed fibers.

### 4.1.3.6    Modeling of mechanical response

In order to compare the goodness of the obtained experimental results with the theoretical previsional models, the empirical equations (3 – 5) to predict the elastic modulus ($E_R$) of a composite containing short-fibers randomly oriented in a plane were used.

A plot of $E_R$ values estimated in accordance with equations (3), (4) and (5) and the experimental results as a function of the fiber volume fraction is reported in figure 24(a). It is worthwhile to note that fiber weight and volume fractions assume the same value for SPCs since fiber and

matrix have the same density. It can be observed that the experimental results in terms of tensile modulus are quite far from that $(E_R)$ predicted for a composite material containing short fibers randomly distributed in a plane (2D). The empirical equations (3 – 5) used to obtain the $E_R$ values are based on a two-dimensional composite and valid only at low fiber volume fraction. At high fiber volume fractions the predicted modulus is much higher than the experimental one due to the increase in concentration of defects within the composite as the content of fibers increases [105]. Moreover, the fibers inside the composites produced in this work are randomly oriented through all the composite volume, in other words the reinforcement present a three dimensional (3D) orientation.

A plot of $E_R$ value according to the Lavengood-Goettler empirical equation (6), Christensen and Waals' model for composites containing short fibers randomly distributed on the volume (equation 7) and the experimental results as a function of the fiber volume fraction is reported in figure 24(b). The experimental value of the elastic modulus of the composite containing only annealed fibers is quite far from the predictions due to its poor interfacial adhesion, once added the coupling agent for composites containing 20 wt% of reinforcement the value increased but still does not achieve its predicted values. On the other hand the SPMC reinforced with plasma treated annealed fibers reached the theoretical $E_R$ values proposed by Christensen and Waals and are quite close to the values predicted using the model proposed by Lavengood and Goettler, attesting once again the effectiveness of the plasma treatment over the annealed fibers.
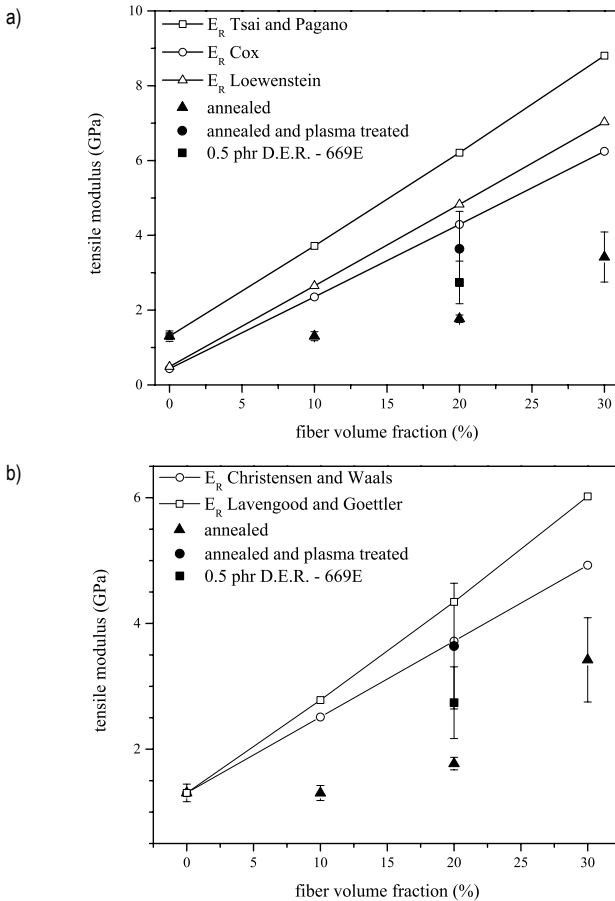
**Figure 24 –** Tensile modulus of SPMCs containing (▲) annealed, (●) plasma treated annealed Vectran® fibers and (■) annealed fibers and 0.5 phr of D.E.R. – 669E. Lines refer to predictive models of equations 3 to 5 (a) and Christensen-Waals and Lavengood-Goettler models (b).

## 4.2 Single polymer nano composites (SPNCs)

As for SPMCs, in order to produce SPNCs a difference in terms of melting temperature and mechanical properties between matrix and reinforcement is required. In this particular case, there are no previous works regarding the production of Vectran® nanofibers. The solution electrospinning technique

was chosen to produce them due to its great flexibility and excellent results in the production of homogeneous non-woven mats.

### 4.2.1    Preparation of Vectran® nanofibers

#### 4.2.1.1    Optimization of electrospinning conditions

Due to one of the main characteristics of Vectran®, its very good chemical resistance, it is quite difficult to produce a homogeneous solution. In order to avoid the use of strong acids at elevated temperatures, a solution of PFP/chloroform (30/70) was used, achieving a maximum solubility of 2.5 wt% of Vectran®. The efficacy of this mixture as a solvent for Vectran is documented in the scientific literature [106]

Then, electrospinning of pure Vectran® NT solution was attempted. The results are presented in the SEM images (Figure 25). It is revealed that using electrospinning of pure Vectran® solution, continuous and uniform nanofibers could not be achieved. This result stems from different factors. The rigid molecular structure of Vectran® results in a limited viscoelastic behavior, which is the primary condition for spinnability in electrospinning [19-21]. The situation is worsened because of the tendency of LCP to form aggregates after a fast evaporation of one of the solvents present in the Vectran® solution (chloroform) [14]. The insufficient spinnability results in rupture of electrospun Vectran® jet producing a mix of dried beads and non-continuous fibers of varying diameters and shapes (figure 25). Several different Vectran® solutions with concentrations in the range 0.5 to 2 wt% have been used in these experiments, as well as different ratios of chloroform/PFP were attempted. In figure 25 it is possible to see that the form and non-uniformity remains unchanged with the increase of Vectran® concentration on the solution.
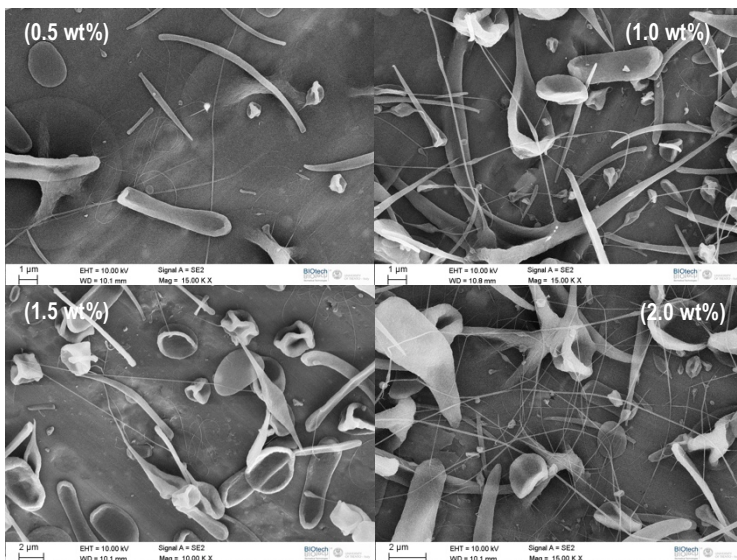
**Figure 25 –** FESEM images of electrospun Vectran® at different concentrations.

The use of spinnable additives, a procedure known as host-guest approach [107], became necessary in order to achieve good quality Vectran®-based nanofibers. Poly(ethylene oxide) was chosen as a "host", since it is a flexible high-molecular-weight polymer widely used to enhance solution viscoelasticity and spinnability. Moreover, PEO is also soluble in chloroform, one of the solvents used in the Vectran® solution. Due to its high molecular weight, a sufficient spinnability was achieved even at relatively small concentrations of PEO (1.85 wt%). This facilitates the subsequent removal of PEO from nanofibers without changing their morphology as showed in the next sections.

The PEO solution was added to the Vectran® solution in different weight ratios, with 1:15 being the most effective, and the resulting nanofibers had a Vectran®/PEO weight ratio of 8.19:1.

### 4.2.1.2   Microstructure

In figure 26(a) continuous nanofibers electrospun from PEO/Vectran® blend are presented. Their average diameter is 195 nm and the molar ratio Vectran®/PEO is 1.25.

After electrospinning of PEO/Vectran® solutions, the resulting nanofiber mats were dried for 24 h at room temperature to remove chloroform completely. After that, only PFP, PEO and Vectran® remain in the fibers. In previous works dealing with Vectran® solutions, dichloromethane (DCM) was used to extract PFP from the film produced [106]. Due to the presence of PEO, DCM could not be used in the present work. In order to remove PEO after fiber formation, the nanofiber mats were immersed for 24 h into a bath containing ethanol and water. In figure 26(b) the Vectran® fibers seem to be swollen in comparison to figure 26(a), partly due to the expected dissolution of PEO after the immersion into water/ethanol bath, and partly due to the plasticizing effect of water absorption. The latter means that water remains entrapped between the Vectran® and the remnant PEO macromolecules in the nanofibers causing an increase in the fibers diameter. Despite the reduction of the PEO content in the nanofibers, to be confirmed using thermogravimetric analysis, the immersion in the water/ethanol bath does not completely eliminate PEO from the nanofibers.

Therefore, instead of using a solvent-based PEO removal procedure, a heat treatment, to be detailed further on, was used to ensure complete removal of PEO from nanofibers, as well as to enhance their thermal stability and mechanical properties. In figure 26(c) the heat-treated nanofibers, which were not immersed in the water/ethanol bath, are seen to be continuous and uniform. On the other hand, in figure 26(d) the nanofibers, which were heat treated after the immersion into the water/ethanol bath, looks melted. Figure 26(b) demonstrates that the fiber mat swells after the immersion into water/ethanol bath, and then, perhaps, partially melts during heat treatment. As a result, nanofibers are additionally sintered, with the average diameter increasing to about 1 $\mu$m.
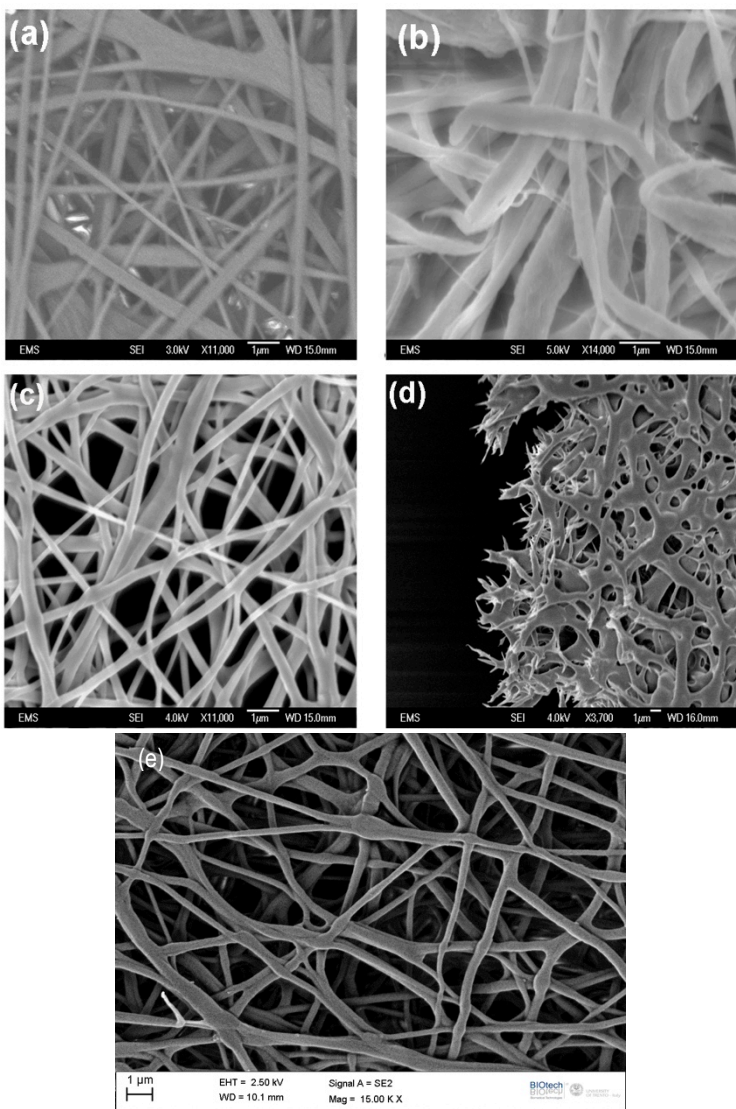
**Figure 26 –** SEM images. (a) Electrospun Vectran®/PEO mat. (b) Electrospun Vectran®/PEO mat after the immersion into water/ethanol bath to dissolve PEO. (c) Heat-treated electrospun Vectran®/PEO fibers. (d) Electrospun Vectran®/PEO mat after immersion into a water/ethanol bath and subsequent heat-treatment. (e) Electrospun Vectran®/PEO mat after heat treatment and subsequent immersion into a water/ethanol bath.

To demonstrate that the swelling was due to the presence of PEO and not related to Vectran® itself, the same immersion procedure was applied to electrospun mats after heat treatment. Figure 26(e) shows that, indeed, no swelling is visible in heat-treated Vectran® nanofiber mats.

### 4.2.1.3   Thermal analysis

To investigate whether the heat treatment resulted in a complete removal of PEO or not, both TGA and DSC techniques have been adopted. The partial dissolution of PEO present in the nanofibers after the immersion into water/ethanol bath was also confirmed by TGA analysis. Degradation of PEO occurs in the range from 200 °C to 420 °C as it can be seen in its thermogravimetric curve (figure 27).
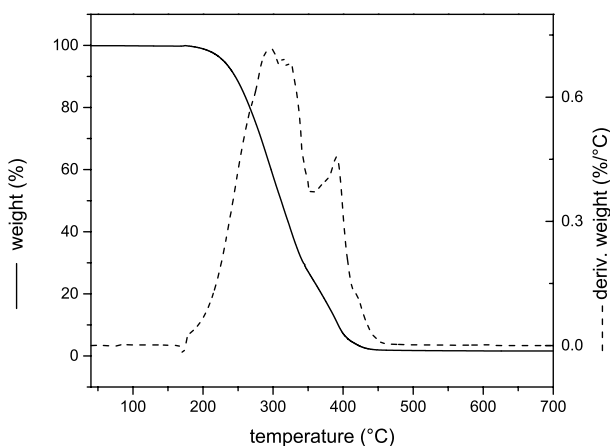


**Figure 27 –** Thermogravimetric curve of as-received PEO ($M_w$=600 kDa).

TGA curves of the electrospun mats reported in figure 28 show that the non-treated nanofibers that were not immersed into the water/ethanol bath lose 14.56% of their weight at 420 °C, while non-treated nanofibers immersed in the bath lose 6.76% in weight at the same temperature. Also, the heat-treated nanofibers that were immersed into the water/ethanol bath loses 1.46%, and the heat-treated nanofibers that were not immersed into the bath lost 1.38%. This slight difference in the weight loss could be explained by the different morphologies of the two mats, namely, a merged

morphology after the immersion and non-merged nanofibers without immersion. The merging results in different surface areas and different amounts of energy required for the Vectran® degradation. The commercial Vectran® NT shows a higher weight loss (3.31%) in comparison with the treated mats, as showed in figure 28.

This higher loss is probably related to the size effect of the commercial fibers, and also to the lower thermal stability of Vectran® NT without the annealing treatment. Our results confirm that the immersion alone is not enough to completely remove PEO from LCP nanofibers. However, after the heat treatment there are no traces of residual PEO in the nanofibers. It can be seen that immersion followed by heat treatment resulted in more conglutinated fibers with larger diameter, and requires additional treatment steps. That is why the immersion stage was completely excluded and the nanofibers of Vectran®/PEO blend were only heat treated to eliminate PEO.

Vectran® begins loosing weight at 460 °C when the first vibrations of the aromatic rings occur. These vibrations continue approximately until 500 °C, which is about 40 °C below the temperature of maximum weight loss of Vectran®. From 510 °C onward there are C–O, O–H and C–H vibrations causing the actual degradation of Vectran®. According to the existing scientific literature, the total degradation of Vectran® completes at about 800 °C [42]. Explaining the further weight loss, observed in figure 28, of all Vectran based materials.

Even though TGA analysis conclusively proves a complete removal of PEO from the blended fibers, a question that still remains is how the heat treatment has influenced the crystalline structure of the electrospun composite nanofibers. As previously described in the section 4.1.1, the presence of two wide endothermic peaks ($Tp_1$, $Tp_2$) in the as-received Vectran® NT can be seen in the DSC thermograms (figure 10(a-b)), which are attributed in the literature to an orthorhombic to nematic transition [9-11,83], after the annealing treatment, a new endothermic peak ($Tm_1$) appears, which overlaps with the two endothermic peaks ($Tp_1$, $Tp_2$) present in the untreated fibers, and becomes a new melting temperature for such fibers [11,83,108,109].
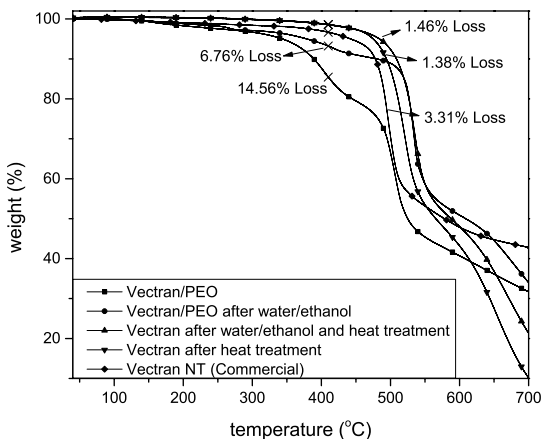
**Figure 28 –** Comparison of TGA data of Vectran®/PEO mat, Vectran®/PEO mat after immersion into water/ethanol bath, Vectran®/PEO mat after heat treatment, and Vectran® NT (commercial).

Initially, the annealing of the nanofibers mats was performed in nitrogen atmosphere at 300 °C for 15 h to mimic a route previously used to anneal Vectran® microfibers. On a visual inspection, nanofibers showed a typical color change. However, the observations with an optical microscope revealed that the nanofiber mat has melted and lost its fibrillar structure. This can be attributed to the fact that due to the smaller diameter of nanofibers, they have a higher surface area/volume ratio in comparison with microfibers. As a result, they melt at a temperature lower than the macro- and microscopic samples of the same polymer, as it was previously demonstrated with other nanofibers [86]. In order to avoid nanofiber melting and merging, the heat treatment temperature was reduced and its duration increased. This annealing procedure was conducted at 250 °C during 24 h in air. The nanofibers showed the expected color change, whereas the optical microscope observations did not reveal any loss in their fibrillar structure.

Figure 29(a) shows the DSC curve of the PEO as-received. It is possible to note a big endothermic peak at around 66 °C that correspond to its melting temperature.

In Figure 29(b) DSC traces of Vectran®/PEO electrospun nanofibers are reported for two cases, before and after heat treatment. The DSC curve

of the untreated Vectran® nanofibers show an endothermic peak at 61.4 °C, related to PEO's melting point, confirming once again its presence in nanofibers before heat treatment. The $Tp_1$ peak found in the untreated microfibers is significantly smoothened out, and the $Tp_2$ peak has disappeared. These peaks are related to a change in the crystallographic phases of Vectran®, and their smoothening could be explained by the presence of PEO, which does not allow the orthorhombic to nematic transitions in the LCP.

After the heat treatment, the peak known as $Tm_1$ appears in the DSC traces of the nanofibers. Also, one of the two endothermic peaks ($Tp_2$) characteristic of Vectran® microfibers appears, indicating the presence of a crystalline structure and a possible orthorhombic to nematic transition. The peak related to PEO is not present anymore, which confirms once again its complete elimination from the nanofibers.

60

b)
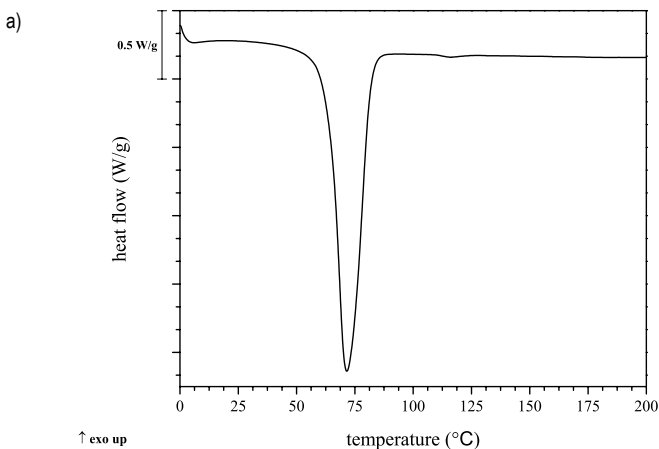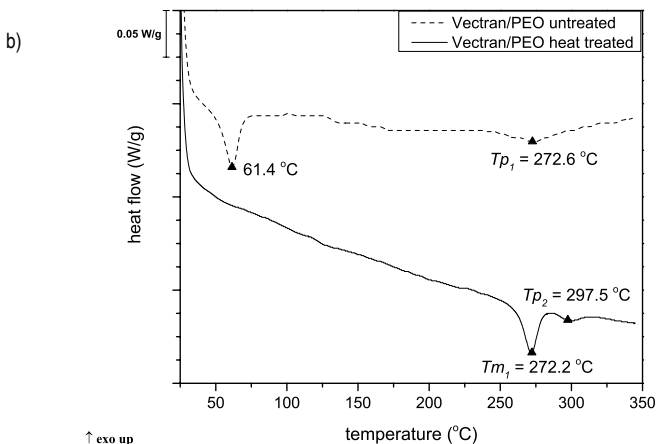
Figure 29 – DSC traces (a) PEO as-received and (b) comparing Vectran® nanofibers before and after heat treatment.

It is emphasized that the $Tm_1$ peak does not overlap the two endothermic peaks as it happens in the commercially available microfibers subjected to a similar heat treatment (Figure 10(b)). The temperature corresponding to the $Tm_1$ peak in the nanofibers is 272.2 °C, which is lower by 38.7 °C than the corresponding peak in the microfibers. According to the previous studies, this phenomenon could be explained mainly by the following three factors: (i) a higher surface area/volume ratio in comparison with microfibers; (ii) plasticizing effect due to a residual solvent; (iii) modification of the crystalline structure as a result of rapid solidification of polymer solutions in electrospinning [86]. The hypothesis of residual solvent can be discarded since TGA and DSC analyses did not show any traces of it. Vectran® is a liquid crystalline polymer, which means that it does not loose its crystalline structure in the liquid phase. From the SAED pattern, to be presented and discussed further on, it could be seen that the presence of PEO, causes the loss of the Vectran® crystalline structure before heat treatment. It will also be demonstrated that although after the heat treatment the nanofibers reveal an increase in their crystalline orientation, their crystalline structure is still not absolutely identical to the commercial Vectran® fibers. The latter possess a higher order in their crystalline structure due to the production process. Therefore, the modification of the crystalline structure due to the fast evaporation of solvents stems from the

61

higher surface area/volume ratio in nanofibers in comparison with microfibers. That increases the propensity to heat dispersion in the nanofibers and could explain the lower temperature of the $Tm_1$ peak in comparison with the position of the same peak in the annealed commercial fibers.

### *4.2.1.4    Infrared spectroscopy*

Also FTIR technique was used in order to ensure the completely PEO removal after the heat treatment. The figure 30 shows the FTIR spectra for the pristine materials (PEO and Vectran NT), the produced nanofiber mat before the heat treatment and the produced nanofiber mat after heat treatment. The main absorbance peaks of Vectran NT were already discussed in the section 4.1.1. Among the peaks present in the pristine PEO spectra it is possible to assign the two with higher absorbance, at 1101 cm$^{-1}$ there is the biggest peak in PEO and represent a C–O–C stretch and at 2885 cm$^{-1}$ that represent a symmetric C–H stretching of CH$_2$ [110]. On the nanofiber mats before the heat treatment it is possible to see the presence of both PEO peaks (1101 cm$^{-1}$ and 2885 cm$^{-1}$) confirming its presence inside the nanofibers before the heat treatment. After the heat treatment both PEO peaks disappear remaining only the characteristic peaks of Vectran pristine fibers, confirming again the completely removal of PEO from the nanofibers produced.
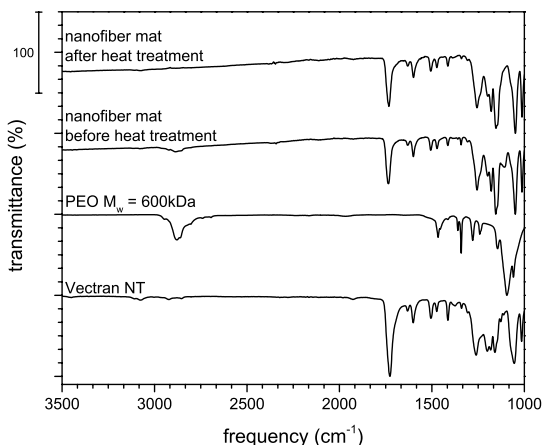
**Figure 30 –** FTIR spectra of pristine PEO and Vectran NT and produced nanofiber mats before and after heat treatment.

### 4.2.1.5    Selected area electron diffraction (SAED)

Although thermal analysis clearly indicates the change in the crystalline order, the final clarification can only be obtained through the experimental evaluation of *d-spacing* in the nanofibers. It should be mentioned that instead of wide-angle X-ray diffraction (WAXD) on nanofiber mats, selected area electron diffraction (SAED) on a single nanofiber was preferred. It was done with the goal to check whether SAED of any arbitrary nanofiber at any location reproduces the same *d-spacing*, as that of annealed Vectran® [50,89,111,112]. Only then it could be concluded that every single nanofiber underwent the lateral packing of crystalline structure. SAED was performed on both untreated and heat-treated Vectran® nanofibers, and some representative images are reported in figure 31. It can be seen from figure 31(a) that the SAED pattern of an untreated nanofiber does not show any sharp ring. The presence of a diffused halo clearly indicates that the existence of PEO had hampered lateral packing thus yielding to an amorphous structure. Otherwise, meridional and equatorial reflections would be visible [50,89,111,112].

63
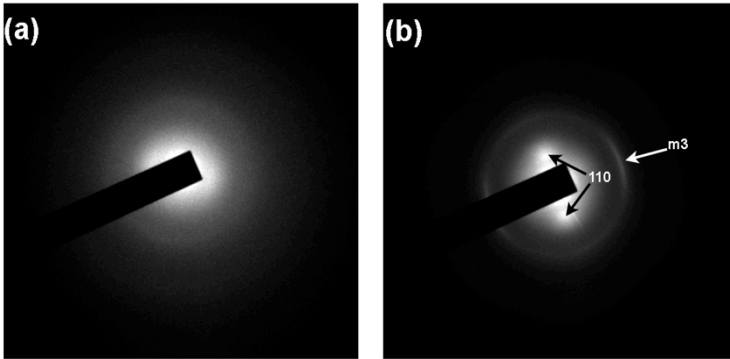
**Figure 31 –** SAED pattern for (a) Vectran® nanofibers before, and (b) after heat treatment. The camera distance was 40 cm in both cases.

In Figure 31(b) the SAED patterns show a strong meridional reflection and one strong equatorial reflection. From the calculation of the *d-spacing* it was found that the *d-spacing* corresponding to the meridional and equatorial reflections was 2.2 Å and 4.7 Å, respectively. According to Kalfon-Cohen et al. [111] Vectran® should have three meridional reflections at the *d-spacings* ~6.73 (*m1*), 3.06 (*m2*) and 2.07 (*m3*) Å. However, the intensity of *m1* and *m2* is quite low and if they would be visible in the SAED pattern, they should have been near the center [111]. The electron beam is so bright that in spite of using a beam stopper, the CCD camera was completely blinded near the center, which makes observation of *m2* and *m1* impossible. The d-spacing value clearly shows that the meridional reflection corresponds to *m3* [111]. Besides the *d-spacing*, the equatorial reflection also shows that it corresponds to 110 plane [111]. The latter, in conjunction with the thermal analysis, conclusively point out that annealing not only destroyed PEO but also improved the lateral order of the random crystal orientation. Also, the random sequences were crystallized into ordered crystals with higher melting temperatures. The increase in the thermal stability after annealing is strongly related to the enhancement of structural order [112]. The existence of an almost circular *m3* ring (with a mix of bright and fading part) in figure 23(b) instead of the arches seen in [111], clearly shows that in our case the crystallites responsible for the *m3* ring are not absolutely aligned the nanofiber axis. However, it can be seen from figure 23(b) that *m3* is brightest in the longitudinal direction of the nanofibers, and

the bright 110 plane is almost at the right angle to it, which appears to be the preferential direction of the crystallite orientation.

### 4.2.1.6    Mechanical properties

Heat treatment is intended not only to remove residual PEO and improve thermal stability of Vectran®, but also to increase mechanical properties of Vectran® nanofibers. According to the previous section (4.1.1), the mechanical properties of Vectran® microfibers are markedly different before and after annealing. The data in table 6 shows that the heat treatment of Vectran® nanofiber mats increased tensile strength by 334% and the elongation at break by 158% in comparison with the untreated nanofiber mats. On the other hand, the tensile modulus of the mats does not change significantly, which is similar to the results obtained after annealing of Vectran® microfibers. Due to the impossibility of using an extensometer directly on the nanofiber mats, the elastic modulus was corrected by taking the machine compliance into account.

**Table 6 –** Tensile properties of heat-treated and untreated Vectran® nanofiber mats.

| Property | Vectran®/PEO untreated | Vectran®/PEO heat-treated |
|---|---|---|
| Tensile modulus [MPa] | 29.5 ± 15.5 | 29.8 ± 10.0 |
| Tensile strength [MPa] | 0.96 ± 0.34 | 4.17 ± 2.2 |
| Elongation at break [%] | 3.01 ± 0.80 | 7.77 ± 2.4 |

In the same way that happens in the microfibers, the improvement in the mechanical properties of the nanofiber mats after a heat treatment has generally been attributed to an increase in Vectran® molecular weight and also to an increasing of alternating copolymer sequences [9,11].

It is emphasized that PEO initially present in the nanofibers before the heat treatment acts as a plasticizer and results in ductile behavior of the untreated mats (figure 32). However, after the annealing when PEO has been completely removed, the nanofiber mats become much stiffer (figure 32), which was the main goal of this heat treatment. Although, the mat strength is smaller than that for individual heat-treated Vectran® microfibers (1.52 ± 0.12 GPa) presented in section 4.1.1, one should keep in mind that tensile strength of nanofiber mats is always much lower than that of an

individual nanofiber [19,113]. The main reasons are that (i) nanofibers in electrospun mats are randomly oriented and cannot be deformed only along their main axis as is commonly done when single microfibers are tested; (ii) the real cross-section of electrospun mats is difficult to be assessed and an average value is generally considered by measuring the external dimensions with a caliper; (iii) while measuring tensile strength of the nanofiber mats, we also inevitably measure effective strength of the inter-fiber bonds, since in the electrospun mats fibers are ill-entangled; (iv) electrospun nanofibers can possess significant porosity due to solvent evaporation and PEO removal. Overall, the factors listed as (i) to (iv) yield mats with a much lower tensile strength than individual nano- and microfibers.
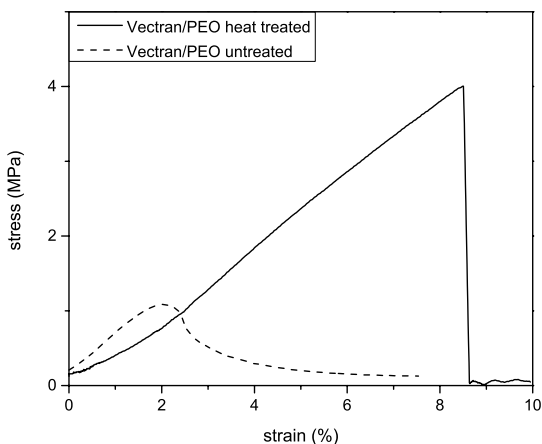


**Figure 32 –** Representative stress-strain curves of heat-treated and untreated Vectran®/PEO nanofiber mats.

Once the Vectran® electrospun nanofiber mats were prepared the SPNCs were produced.

### 4.2.2    SPNCs characterization

The consolidation route for the single polymer nano composites was developed adapting the film-stacking process to the special characteristics

required for the use of Vectran® nanofiber as reinforcement and is described in the section 3.2.2.1

### *4.2.2.1    Microstructure*

Figure 33 shows the debonding of the two matrix plates of the SPNC unfilled matrix, which can cause the premature failure of the sample and a further reduction of its mechanical properties.



**Figure 33 –** Micrograph of SPNCs matrix debonding after the consolidation.

This behavior can explain how the nanofiber mats, even having a smaller tensile modulus than the unfilled matrix, can improve the tensile modulus of the SPNCs. Having a higher surface area and a lower melting temperature than the matrix plates, the nanofiber mats act as an adhesive, bonding both plates forming a composite. It is interesting to note that the standard deviation of the composites mechanical properties (table 7) is notoriously smaller in comparison with the unfilled matrix.  Figure 34 shows that there is no debonding after the addition of the nanofiber mats.
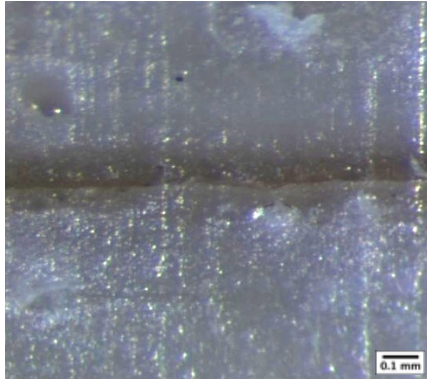
**Figure 34 –** Micrograph of SPNC containing 10 vol% of nanofibers.

FESEM images of the unfilled matrix and SPNC containing 10 vol% are presented in figure 35. The unfilled matrix, on figure 35(a), revealed the normal behavior of Vectran® fracture, and did not present any signal of nanofibers presence; in addition, it is not possible to see any difference in the junction of the two plates. In figure 35(b) it is possible to note the presence of the nanofibers due to a line at the junction of the two matrix plates, region in which the nanofiber mats were placed, this line shows that there is an interaction of the nanofibers with the two plates. The figure 35(c) shows a micrograph with a higher magnification of the junction area; unfortunately, the Vectran® fracture generates several microfibrils, and even at this higher magnification it is not possible to visualize the nanofibers inside the material.
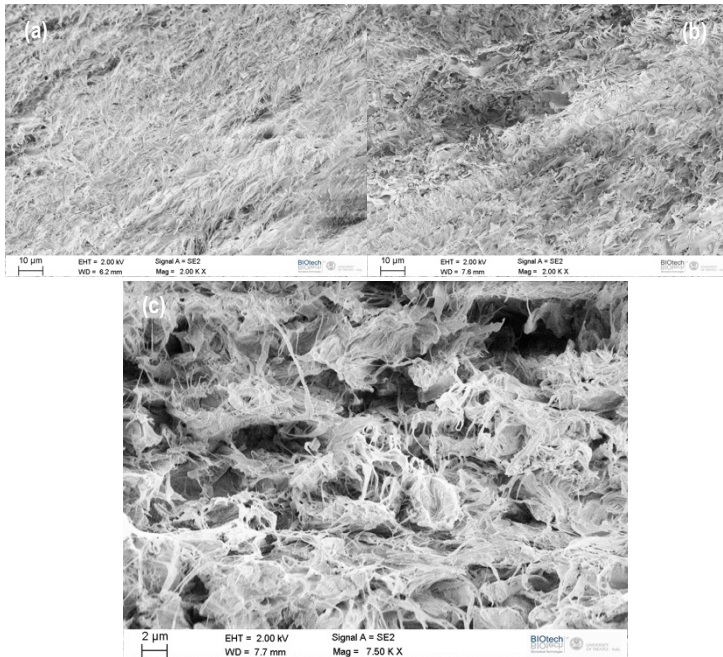
**Figure 35 –** FESEM micrographs of a) unfilled matrix, b) SPNC with 10 vol% and c) higher magnification of the SPNCs' junction area.

### 4.2.2.2    Thermal analysis

In order to confirm the presence of the nanofiber mats in the SPNCs after the consolidation, DSC technique was performed and their curves can be seen in figure 36. In the unfilled matrix it is possible to found two endothermic peaks, the first one with larger enthalpy at around 280 °C is related to the melting temperature of the matrix, mimicking the literature behavior [111]. The matrix suffered two pressing, the first one to be transformed from fibers to thin plates and the second to consolidate the composite. The second peak, at around 294 °C, can be tentatively explained by a new "heat treatment" suffered by the matrix during the composites processing route. In the SPNC containing 10 vol% of nanofibers it is possible to note the presence of three peaks, the first one at around 280 °C that correspond to the melting temperature of the Vectran® matrix as mentioned earlier; the second peak (around 293 °C) is related to a "heat

69

treatment" induced to the matrix during the composite preparation. The third one, at around 304 °C could be related a new "heat treatment" induced on the nanofiber during the composites consolidation.
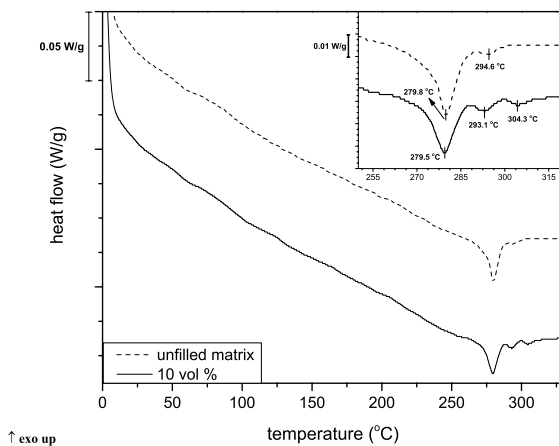


**Figure 36 –** DSC curves of unfilled matrix and SPNCs containing 10 vol%.

The DSC technique was used also to prove the recyclability of the SPNC. The curve of the second scanning (figure 37), after a total melting of the composite, shows only one peak instead of the three present on the first scan of the composite. This peak appears around 284 °C, mimicking the behavior of SPMCs (section 4.1.2.3), and can be used as indication that the material does not present any fibers inside it. The temperature of the new peak it is a strong indication that the material does not show any thermodynamic signal of degradation and can be considered fully-recyclable, confirming the main idea of the SPCs.
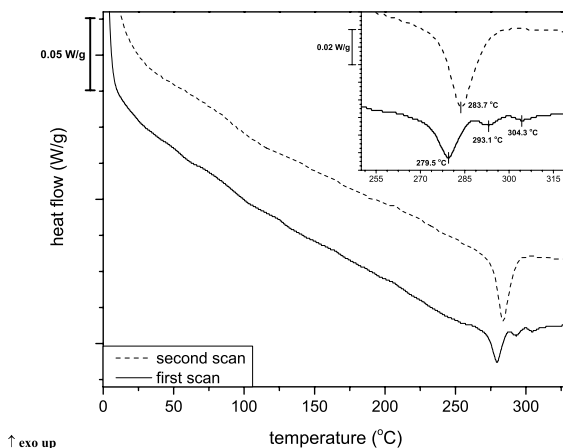
**Figure 37 -** DSC curves of unfilled matrix and SPNCs containing 10 vol%.

### 4.2.2.3 Mechanical properties

The results of the tensile tests on the SPNCs are compared in table 7 and an example of their stress-strain curve is draw in figure 38.

It is possible to note that the addition of 10 vol% of nanofibers increased the tensile modulus in about 18% in comparison with the unfilled matrix. In the same way, the tensile strength increased of about 19% without significantly changes in the elongation at break of the composite. One should keep in mind that the nanofiber mats have a very lower value of mechanical properties in comparison with a single filament of commercial fibers, and even with lower mechanical properties it was possible to increase the mechanical properties of the unfilled matrix by the addition of 10 vol% of nanofibers.

**Table 7 -** Tensile properties of unfilled matrix and SPNCs containing 10 vol%.

| Property | Unfilled Matrix | SPNCs 10 vol% |
|---|---|---|
| Tensile modulus [MPa] | 730.2 ± 156.3 | 862.8 ± 22.4 |
| Tensile strength [MPa] | 14.1 ± 2.4 | 16.8 ± 1.0 |
| Elongation at break [%] | 2.28 ± 0.18 | 2.33 ± 0.14 |
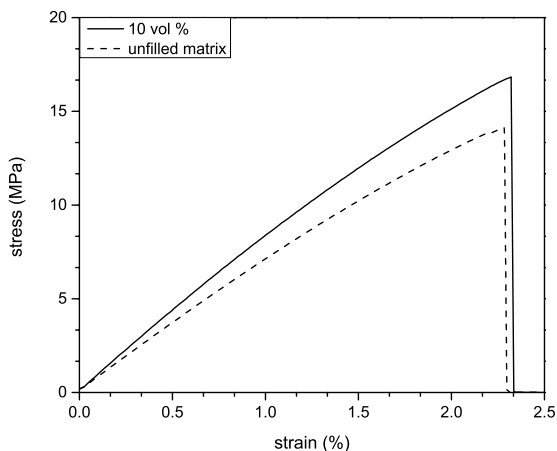
**Figure 38 –** Representative stress-strain curves of unfilled matrix and SPNCs containing 10 vol%.

Due to the difference on processing in comparison with the unfilled matrix of SPMCs, the latter prepared by simple hot-pressing and the first by pressing two plates at a lower temperature, the mechanical properties are markedly lower, as reported in table 8, in the case of SPNCs.

**Table 8 -** Tensile properties of SPMCs unfilled matrix and SPNCs unfilled matrix.

| Property | Unfilled Matrix SPMCs | Unfilled Matrix SPNCs |
|---|---|---|
| Tensile modulus [MPa] | 1310.3 ± 140.1 | 730.2 ± 156.3 |
| Tensile strength [MPa] | 37.7 ± 9.2 | 14.1 ± 2.4 |
| Elongation at break [%] | 5.00 ± 1.44 | 2.28 ± 0.18 |

Unfortunately, as described in the previous section (4.2.1.3), the heat treatment over the nanofiber mats does not improve their melting temperature, becoming impossible to mimic the consolidation processing of SPMCs.

# CONCLUSIONS

Single polymer composites using micro- and nano- fibers as reinforcement were successfully prepared starting from Vectran® fibers and had been characterized using multidisciplinary techniques.

In the first part of the thesis work, an annealing treatment over the commercially available microfibers was optimized in order to improve their thermal stability and the mechanical properties. An increase of more than 35% on tensile strength without reducing the tensile modulus was achieved. The melting temperature of the fibers increased by almost 30 °C, thus allowing the production of short fiber reinforced single-polymer composites (SPMCs).

With 20 and 30 wt% of reinforcement SPMCs showed a improvement of the dynamic-mechanical properties. Unfortunately FESEM micrographs revealed the presence of diffuse pull-out phenomena evidencing a poor interfacial adhesion between fibers and matrix. A reactive compatibilization using an epoxy resin was investigated, and at low amount (0.5 phr) of coupling agent improved by 55% the tensile modulus. Increasing the amount of coupling agent agglomeration phenomena were noticed, causing premature failure of the composites. In order to improve the interfacial adhesion without the addition of coupling agents, a plasma surface treatment was attempted. The SPMC containing 20 wt% of plasma treated fibers improved their tensile modulus by a remarkable extent (178%) in comparison with the unfilled matrix. FESEM micrographs confirmed the effectiveness of plasma surface treatment. In fact, diffuse fiber breakage phenomena were observed which is an indirect proof of an improvement of the fiber-matrix interfacial adhesion.. DSC and FTIR analyses were used in order to verify the recyclability of the produced SPMCs. It was found that the SPMCs did not suffer any thermal and chemical changes after melting, thus confirming the SPC concept.

In the second part of the thesis work, electrospinning technique was used to produce Vectran® nanofibers. Due to its rigid chemical structure, an "host-guest" approach (using PEO as host) have been adopted. In this way, electrospun mats containing Vectran®/PEO nanofibers were produced. A heat-treatment was optimized to remove the remaining PEO and improve

the thermal stability and mechanical properties of the nanofibers. DSC, TGA and FTIR concurrently proved the complete removal of PEO after the heat-treatment. Tensile tests revealed a remarkable improvement of 334% of the heat-treated mats tensile strength in comparison with the untreated ones. Also, a change of the mechanical behavior from ductile to brittle was found. SAED technique confirmed the improvement of the lateral order of the random crystal orientation. However, the thermal treatment did improve the melting temperature by a very low amount.

Due to the small processing window in terms of melting temperature between matrix and reinforcement, an adapted film-stacking technique was used to consolidate the SPNCs. The composite containing 10 vol% of nanofibers showed an increase of about 20% in the tensile modulus and tensile strength. DSC and FESEM micrographs confirmed the presence of the nanofibers in the final composite. Moreover, DSC was used to check the recyclability of the SPNCs showing that the polymer does not suffer of degradative effects, thus confirming the SPC concept.

The SPMCs manifested better mechanical properties compared with the SPNCs. This can be explained by several reasons: i) the adapted film-stacking process chosen to consolidate the composites caused the presence of trapped air-bubbles; ii) the sandwich structure of the obtained composites generated a force concentration in the junction of the plates causing a premature failure of the composite; iii) the nanofiber mat could not be totally embedded by the matrix as it happens with the reinforcement in the SPMCs. Further works on SPNCs could include the addition of small quantity of additives (e.g. carbon nanofibers, graphene, intrinsic conductive polymers) in order to functionalize the composite generating sensors or even self-healing SPNCs.

Nowadays, composite materials are widely used in automotive and aeronautic industries. Thermoplastic composites reinforced with glass and carbon fibers have good mechanical properties coupled with low density compared with metals and thermoset composites, however does not present the required recyclability. The SPMCs developed in this work could open a new avenue in the field of thermoplastic composites, coupling the good mechanical properties and low density with a complete recyclability.

# REFERENCES

[1]     Pegoretti, A., *Editorial corner – a personal view. Trends in composite materials: the challenge of single-polymer composites*. Express Polymer Letters, **2007**, 1: p. 710-710.

[2]     Matabola, K. P., A. R. De Vries, F. S. Moolman and A. S. Luyt, *Single polymer composites: a review*. Journal of Materials Science, **2009**, 44: p. 6213-6222.

[3]     Pegoretti, A. and M. Traina, 12, in Handbook of tensile properties of textile and technical fibres, ed. A.R. Bunsell, **2009**, Woodhead Publishing Ltd: Cambridge, UK, p. 354-436.

[4]     Donald, A. M., A. H. Windle and S. Hanna, *Liquid crystalline polymers*. **2006**: Cambridge University Press.

[5]     Wang, X., Q. F. Zhou and Q. Zhou, *Liquid crystalline polymers*. **2004**: World Scientific Pub. Co.

[6]     Pegoretti, A., A. Zanolli and C. Migliaresi, *Flexural and interlaminar mechanical properties of unidirectional liquid crystalline single-polymer composites*. Composites Science and Technology, **2006**, 66: p. 1953-1962.

[7]     Pegoretti, A., A. Zanolli and C. Migliaresi, *Preparation and tensile mechanical properties of unidirectional liquid crystalline single-polymer composites*. Composites Science and Technology, **2006**, 66: p. 1970-1979.

[8]     Isayev, A. I., *Self-reinforced composites involving liquid-crystalline polymers - Overview of development and applications*. Liquid-Crystalline Polymer Systems, **1996**, 632: p. 1-20.

[9]     Sarlin, J. and P. Tormala, *Heat-Treatment Studies of a Tlcp Fiber*. Journal of Applied Polymer Science, **1993**, 50: p. 1225-1231.

[10]    Sarlin, J. and P. Tormala, *Isothermal Heat-Treatment of a Thermotropic Lcp Fiber*. Journal of Polymer Science Part B-Polymer Physics, **1991**, 29: p. 395-405.

[11]    Kalfon-Cohen, E., A. Pegoretti and G. Marom, *Annealing of drawn monofilaments of liquid crystalline polymer vectra/vapor grown carbon fiber nanocomposites*. Polymer, **2010**, 51: p. 1033-1041.

[12]    Huang, Z. M., Y. Z. Zhang, M. Kotaki and S. Ramakrishna, *A review on polymer nanofibers by electrospinning and their applications in nanocomposites*. Composites Science and Technology, **2003**, 63: p. 2223-2253.

[13]    Stephens, J. S., D. B. Chase and J. F. Rabolt, *Effect of the electrospinning process on polymer crystallization chain conformation in nylon-6 and nylon-12*. Macromolecules, **2004**, 37: p. 877-881.

[14]    Wu, Y. G., Q. An, J. X. Yin, T. Hua, H. M. Xie, G. T. Li and H. Tang, *Liquid crystal fibers produced by using electrospinning technique*. Colloid and Polymer Science, **2008**, 286: p. 897-905.

[15]    Nakashima, K., K. Tsuboi, H. Matsumoto, R. Ishige, M. Tokita, J. Watanabe and A. Tanioka, *Control over Internal Structure of Liquid*

*Crystal Polymer Nanofibers by Electrospinning*. Macromolecular Rapid Communications, **2010**, 31: p. 1641-1645.

[16] Reneker, D. H. and I. Chun, *Nanometre diameter fibres of polymer, produced by electrospinning*. Nanotechnology, **1996**, 7: p. 216-223.

[17] Srinivasan, G. and D. H. Reneker, *Structure and Morphology of Small-Diameter Electrospun Aramid Fibers*. Polymer International, **1995**, 36: p. 195-201.

[18] Krause, S., R. Dersch, J. H. Wendorff and H. Finkelmann, *Photocrosslinkable liquid crystal main-chain polymers: Thin films and electrospinning*. Macromolecular Rapid Communications, **2007**, 28: p. 2062-2068.

[19] Reneker, D. H., A. L. Yarin, E. Zussman and H. Xu, *Electrospinning of nanofibers from polymer solutions and melts*. Advances in Applied Mechanics, **2007**, 41: p. 43-195.

[20] Reneker, D. H. and A. L. Yarin, *Electrospinning jets and polymer nanofibers*. Polymer, **2008**, 49: p. 2387-2425.

[21] Reneker, D. H., A. L. Yarin, H. Fong and S. Koombhongse, *Bending instability of electrically charged liquid jets of polymer solutions in electrospinning*. Journal of Applied Physics, **2000**, 87: p. 4531-4547.

[22] Mazumdar, S., *Composites Manufacturing: Materials, Product, and Process Engineering*. **2001**: Taylor & Francis.

[23] Nielsen, L. E., *Mechanical Properties of Polymers and Composites: (in Two Volumes)*. **1974**: Marcel Dekker.

[24] Mallick, P. K., *Fiber-reinforced composites: materials, manufacturing, and design*. **2008**: CRC Press.

[25] Koo, J., *Polymer Nanocomposites*. **2010**: McGraw-Hill Education.

[26] Banik, K., T. N. Abraham and J. Karger-Kocsis, *Flexural Creep Behavior of Unidirectional and Cross-Ply All-Poly(propylene) (PURE®) Composites*. Macromolecular Materials and Engineering, **2007**, 292: p. 1280-1288.

[27] Kmetty, Á., T. Bárány and J. Karger-Kocsis, *Self-reinforced polymeric materials: A review*. Progress in Polymer Science, **2010**, 35: p. 1288-1310.

[28] Peijs, T., *Composites for recyclability*. Materials today, **2003**, 6: p. 30-35.

[29] Capiati, N. and R. Porter, *The concept of one polymer composites modelled with high density polyethylene*. Journal of Materials Science, **1975**, 10: p. 1671-1677.

[30] Abo El-Maaty, M. I., D. C. Bassett, R. H. Olley, P. J. Hine and I. M. Ward, *The hot compaction of polypropylene fibres*. Journal of Materials Science, **1996**, 31: p. 1157-1163.

[31] Hine, P. J., I. M. Ward, N. D. Jordan, R. Olley and D. C. Bassett, *The hot compaction behaviour of woven oriented polypropylene fibres and tapes. I. Mechanical properties*. Polymer, **2003**, 44: p. 1117-1131.

[32] Jordan, N. D., D. C. Bassett, R. H. Olley, P. J. Hine and I. M. Ward, *The hot compaction behaviour of woven oriented polypropylene fibres and tapes. II. Morphology of cloths before and after compaction*. Polymer, **2003**, 44: p. 1133-1143.

[33]     Ward, I. M., P. J. Hine and K. Norris, Polymeric materials, GB2253420, **1992**. B.P. Office.

[34]     Ward, I. M. and P. J. Hine, *The science and technology of hot compaction*. Polymer, **2004**, 45: p. 1413-1427.

[35]     Karger-Kocsis, J., *Polypropylene. 1. Structure and morphology*. **1995**: Chapman & Hall.

[36]     Rasburn, J., P. J. Hine, I. M. Ward, R. H. Olley, D. C. Bassett and M. A. Kabeel, *The hot compaction of polyethylene terephthalate*. Journal of Materials Science, **1995**, 30: p. 615-622.

[37]     Li, R. and D. Yao, *Preparation of single poly(lactic acid) composites*. Journal of Applied Polymer Science, **2008**, 107: p. 2909-2916.

[38]     Wright-Charlesworth, D. D., E. P. Lautenschlager and J. L. Gilbert, *Hot compaction of poly(methyl methacrylate) composites based on fiber shrinkage results*. Journal of Materials Science: Materials in Medicine, **2005**, 16: p. 967-975.

[39]     Hine, P. J. and I. M. Ward, *Hot compaction of woven nylon 6,6 multifilaments*. Journal of Applied Polymer Science, **2006**, 101: p. 991-997.

[40]     Matabola, K. P., A. R. de Vries, A. S. Luyt and R. Kumar, *Studies on single polymer composites of poly(methyl methacrylate) reinforced with electrospun nanofibers with a focus on their dynamic mechanical properties*. Express Polymer Letters, **2011**, 5: p. 635-642.

[41]     Friedel, G. États mésomorphes de la matiere. in Annales de Physique. **1922.**

[42]     Chung, T. S., *Thermotropic liquid crystal polymers: thin-film polymerization, characterization, blends, and applications*. **2001**: Technomic Publishing Company.

[43]     Demus, D., J. Goodby, G. W. Gray, H.-W. Spiess and V. V., *Handbook of Liquid Crystals: Fundamentals*. **1998**: Wiley-VCH.

[44]     Gedde, U. W., *Polymer Physics*. **1995**: Springer.

[45]     García, J. M., F. C. García, F. Serna and J. L. de la Peña, *High-performance aromatic polyamides*. Progress in Polymer Science, **2010**, 35: p. 623-686.

[46]     Hearle, J. W. S., *High Performance Fibres*. **2001**: Textile Institute.

[47]     Blackwell, J., A. Biswas and R. C. Bonart, *X-ray studies of the structure of liquid-crystalline copolyesters: treatment of an atomic model as a one-dimensional paracrystal*. Macromolecules, **1985**, 18: p. 2126-2130.

[48]     Hanna, S. and A. H. Windle, *Geometrical limits to order in liquid crystalline random copolymers*. Polymer, **1988**, 29: p. 207-223.

[49]     Biswas, A. and J. Blackwell, *X-ray diffraction from liquid-crystalline copolyesters: matrix methods for intensity calculations using a one-dimensional paracrystalline model*. Macromolecules, **1987**, 20: p. 2997-3002.

[50]     Langelaan, H. C. and A. P. deBoer, *Crystallization of thermotropic liquid crystalline HBA/HNA copolymers*. Polymer, **1996**, 37: p. 5667-5680.

[51]     Muhlebach, A., J. Economy, R. D. Johnson, T. Karis and J. Lyerla, *Direct evidence for transesterification and randomization in a mixture of*

77

homopolyesters of poly(4-hydroxybenzoic acid) and poly(6-hydroxy-2-naphthoic acid) above 450.degree. Macromolecules, **1990**, 23: p. 1803-1809.

[52] Fakirov, S., *Transreactions in Condensation Polymers*. **2008**: Wiley.

[53] Schneggenburger, L. A., P. Osenar and J. Economy, *Direct Evidence for Sequence Ordering of Random Semicrystalline Copolyesters during High-Temperature Annealing*. Macromolecules, **1997**, 30: p. 3754–3758.

[54] Callister, W. D. and D. G. Rethwisch, *Materials Science and Engineering: An Introduction*. **2010**: John Wiley & Sons.

[55] Andrady, A. L., *Science and Technology of Polymer Nanofibers*. **2008**: John Wiley & Sons.

[56] Formhals, A., Process and apparatus for preparing artificial threads, 1975504, **1934**. U.P. Office.

[57] Stanger, J., N. Tucker and M. Staiger, *Electrospinning*. **2009**: Rapra Technology.

[58] Ramakrishna, S., *An Introduction to Electrospinning And Nanofibers*. **2005**: World Scientific.

[59] Lin, T., *Nanofibers-production, properties and functional applications*. **2011**. Rijeka, Croatia: InTech.

[60] Li, D. and Y. Xia, *Electrospinning of Nanofibers: Reinventing the Wheel?* Advanced Materials, **2004**, 16: p. 1151-1170.

[61] Doshi, J. and D. H. Reneker, *Electrospinning process and applications of electrospun fibers*. Journal of Electrostatics, **1995**, 35: p. 151-160.

[62] Yarin, A. L., S. Koombhongse and D. H. Reneker, *Bending instability in electrospinning of nanofibers*. Journal of Applied Physics, **2001**, 89: p. 3018-3026.

[63] Dzenis, Y., *Spinning Continuous Fibers for Nanotechnology*. Science, **2004**, 304: p. 1917-1919.

[64] Bhardwaj, N. and S. C. Kundu, *Electrospinning: A fascinating fiber fabrication technique*. Biotechnology Advances, **2010**, 28: p. 325-347.

[65] Zhang, C., X. Yuan, L. Wu, Y. Han and J. Sheng, *Study on morphology of electrospun poly(vinyl alcohol) mats*. European Polymer Journal, **2005**, 41: p. 423-432.

[66] Demir, M. M., I. Yilgor, E. Yilgor and B. Erman, *Electrospinning of polyurethane fibers*. Polymer, **2002**, 43: p. 3303-3309.

[67] Teo, W. E. and S. Ramakrishna, *Electrospun fibre bundle made of aligned nanofibres over two fixed points*. Nanotechnology, **2005**, 16: p. 1878.

[68] Chang, W. N., *Nanofibers: Fabrication, Performance, and Applications*. **2009**: Nova Science.

[69] Halpin, J. C., *Effects of Environmental Factors on Composite Materials*. **1969**: p.

[70] Halpin, J. C. and K. M. Finlayson, *Primer on Composite Materials Analysis*. **1992**: Technomic Publishing Company.

[71] Hermans, J. J., *The elastic properties of fiber oriented materials when the fibers are aligned*. Koninkl. Nederl. Akademie Van Wetenschappen-Amsterdam, **1967**, 65: p. 1 - 9.

[72]     Hill, R., *Elastic properties of reinforced solids: Some theoretical principles*. Journal of the Mechanics and Physics of Solids, **1963**, 11: p. 357-372.

[73]     Halpin, J. C. and J. L. Kardos, *Halpin-Tsai Equations - Review*. Polymer Engineering and Science, **1976**, 16: p. 344-352.

[74]     Tsai, S. W. and N. J. Pagano, *Composite materials workshop*. **1968**. Stamford, Conn.: Technomic Pub. Co.

[75]     Cox, H. L., *The elasticity and strength of paper and other fibrous materials*. Br. J. Appl. Phys., **1952**, 3: p. 8.

[76]     Loewenstein, K. L., *Composite Materials*. **1966**. New York: Holliday and Elsevier.

[77]     Lavengood, R. E., L. A. Goettler and M. R. C. S. L. MO., *Stiffness of Non-Aligned Fiber Reinforced Composites*. **1971**: Defense Technical Information Center.

[78]     Kardos, J., *Critical issues in achieving desirable mechanical properties for short fiber composites*. Pure and applied chemistry, **1985**, 57: p. 1651-1657.

[79]     Nielsen, L. E., *Morphology and the elastic modulus of block polymers and polyblends*. Rheologica Acta, **1974**, 13: p. 86-92.

[80]     Christensen, R. M., *Mechanics of composite materials*. **1979**: Wiley.

[81]     Christensen, R. M. and F. M. Waals, *Effective Stiffness of Randomly Oriented Fibre Composites*. Journal of Composite Materials, **1972**, 6: p. 518-535.

[82]     Lee, L. H., *Strength -Composition relationships of random short glass fiber -thermoplastics composites*. Polymer Engineering & Science, **1969**, 9: p. 213-224.

[83]     Menczel, J. D., G. L. Collins and S. K. Saw, *Thermal analysis of Vectran(R) fibers and films*. Journal of Thermal Analysis, **1997**, 49: p. 201-208.

[84]     Yoon, H. N., L. F. Charbonneau and G. W. Calundann, *Synthesis, Processing and Properties of Thermotropic Liquid-Crystal Polymers*. Advanced Materials, **1992**, 4: p. 206-214.

[85]     Wang, X. F., J. Engel and C. Liu, *Liquid crystal polymer (LCP) for MEMS: processes and applications*. Journal of Micromechanics and Microengineering, **2003**, 13: p. 628-633.

[86]     Srikar, R., T. Gambaryan-Roisman, C. Steffes, P. Stephan, C. Tropea and A. L. Yarin, *Nanofiber coating of surfaces for intensification of drop or spray impact cooling*. International Journal of Heat and Mass Transfer, **2009**, 52: p. 5814-5826.

[87]     Medeiros Araujo, T., S. Sinha-Ray, A. Pegoretti and A. L. Yarin, *Electrospinning of a blend of a liquid crystalline polymer with poly(ethylene oxide): Vectran nanofiber mats and their mechanical properties*. Journal of Materials Chemistry C, **2013**, 1: p. 351-358.

[88]     van Gulijk, C., K. M. de Lathouder and R. Haswell, *Characterizing herring bone structures in carbon nanofibers using selected area electron diffraction and dark field transmission electron microscopy*. Carbon, **2006**, 44: p. 2950-2956.

[89]     Kalfon-Cohen, E., G. Marom, E. Wachtel and A. Pegoretti, *Characterization of drawn monofilaments of liquid crystalline polymer/carbon nanoparticle composites correlated to nematic order*. Polymer, **2009**, 50: p. 1797-1804.

[90]     Taylor, J. E., A. Romo-Uribe and M. R. Libera, *Molecular orientation gradients in thermotropic liquid crystalline fiber*. Polymers for Advanced Technologies, **2003**, 14: p. 595-600.

[91]     Weibull, W., *A statistical distribution function of wide applicability*. Journal of applied mechanics, **1951**, 18: p. 293-297.

[92]     Asloun, M., J. B. Donnet, G. Guilpain, M. Nardin and J. Schultz, *On the estimation of the tensile strength of carbon fibres at short lengths*. Journal of Materials Science, **1989**, 24: p. 3504-3510.

[93]     Chen, B.-K., S.-Y. Tsay and J.-Y. Chen, *Synthesis and properties of liquid crystalline polymers with low Tm and broad mesophase temperature ranges*. Polymer, **2005**, 46: p. 8624-8633.

[94]     Seidel, C., C. Damm and H. Muenstedt, *Surface modification of films of various high temperature resistant thermoplastics*. Journal of Adhesion Science and Technology, **2007**, 21: p. 423-439.

[95]     Castellano, M., D. Nebbia, A. Turturro, B. Valenti, G. Costa and L. Falqui, *Reactive blending of polyamide 6,6 and Vectra A, 2 - Role of a bifunctional epoxy coupler*. Macromolecular Chemistry and Physics, **2002**, 203: p. 1614-1624.

[96]     Chin, H. C. and F. C. Chang, *Reactive compatibilization of PET/LCP blends by a multifunctional epoxy coupler*. Polymer, **1997**, 38: p. 2947-2956.

[97]     Chin, H. C., K. C. Chiou and F. C. Chang, *Reactive compatibilization of the poly(ethylene terephthalate) liquid crystalline polymer blends by solid epoxy resin as a coupling agent*. Journal of Applied Polymer Science, **1996**, 60: p. 2503-2516.

[98]     Chiou, Y. P., D. Y. Chang and F. C. Chang, *In situ compatibility of polystyrene and liquid crystalline polymer blends*. Polymer, **1996**, 37: p. 5653-5660.

[99]     Chiou, Y.-P., K.-C. Chiou and F.-C. Chang, *In situ compatibilized polypropylene/liquid crystalline polymer blends*. Polymer, **1996**, 37: p. 4099-4106.

[100]    Kaplan, S. L. and P. W. Rose, *Plasma surface treatment of plastics to enhance adhesion*. International Journal of Adhesion and Adhesives, **1991**, 11: p. 109-113.

[101]    Stephen, K. and R. Peter, in Coatings Technology Handbook, Third Edition, **2005**, CRC Press, p. 39-31-39-36.

[102]    Om, K., in Handbook of Adhesive Technology, Revised and Expanded, **2003**, CRC Press.

[103]    Gleich, H., R. M. Criens, H. G. Moslé and U. Leute, *The influence of plasma treatment on the surface properties of high-performance thermoplastic*. International Journal of Adhesion and Adhesives, **1989**, 9: p. 88-94.

[104]    Kalika, D. S. and D. Y. Yoon, *Dielectric relaxation studies of poly(4-hydroxybenzoic acid) and copolyesters based on 4-hydroxybenzoic acid and 6-hydroxy-2-naphthoic acid*. Macromolecules, **1991**, 24: p. 3404-3412.

[105]    Blumentritt, B. F., B. T. Vu and S. L. Cooper, *Mechanical properties of discontinuous fiber reinforced thermoplastics. II. Random-in-plane fiber orientation*. Polym. Eng. Sci., **1975**, 15: p. 428-436.

[106]    Yonetake, K., T. Sagiya, K. Koyama and T. Masuko, *Phase-Transition of Thermotropic Liquid-Crystalline Copolyester Film*. Macromolecules, **1992**, 25: p. 1009-1010.

[107]    Yarin, A. L., E. Zussman, J. H. Wendorff and A. Greiner, *Material encapsulation and transport in core-shell micro/nanofibers, polymer and carbon nanotubes and micro/nanochannels*. Journal of Materials Chemistry, **2007**, 17: p. 2585-2599.

[108]    Medeiros Araujo, T. and A. Pegoretti. Preparation and characterization of liquid crystalline single-polymer short-fibres composites. in XX Convegno Italiano di Scienza e Tecnologia delle Macromolecole. **2011.** Terni, Italy

[109]    Medeiros Araujo, T. and A. Pegoretti. Liquid crystalline single-polymer short-fibers composites. in 15th European Conference on Composite Materials. **2012.** Venezia, Italy

[110]    Yoshihara, T., H. Tadokoro and S. Murahashi, *Normal Vibrations of the Polymer Molecules of Helical Conformation. IV. Polyethylene Oxide and Polyethylene-d[sub 4] Oxide*. The Journal of Chemical Physics, **1964**, 41: p. 2902-2911.

[111]    Kalfon-Cohen, E., G. Marom, A. Weinberg, E. Wachtel, C. Migliaresi and A. Pegoretti, *Microstructure and nematic transition in thermotropic liquid crystalline fibers and their single polymer composites*. Polymers for Advanced Technologies, **2007**, 18: p. 771-779.

[112]    Kaito, A., M. Kyotani and K. Nakayama, *Effects of Annealing on the Structure Formation in a Thermotropic Liquid-Crystalline Copolyester*. Macromolecules, **1990**, 23: p. 1035-1040.

[113]    Zussman, E., M. Burman, A. L. Yarin, R. Khalfin and Y. Cohen, *Tensile deformation of electrospun nylon-6,6 nanofibers*. Journal of Polymer Science Part B-Polymer Physics, **2006**, 44: p. 1482-1489.

# PUBLICATIONS AND CONGRESS PRESENTATIONS

## PUBLICATIONS

Medeiros Araujo, T., S. Sinha-Ray, A. Pegoretti and A. L. Yarin,
**"*Electrospinning of a blend of a liquid crystalline polymer with poly(ethylene oxide): Vectran® nanofiber mats and their mechanical properties.*"**,
*Journal of Materials Chemistry C, 1. (2013) 351 - 358.*

Medeiros Araujo T. and A. Pegoretti,
**"*Liquid crystalline single-polymer short-fibers composites*"**,
*Composite Interfaces.  (2013).*

## CONGRESS PRESENTATIONS

Medeiros Araujo T. and A. Pegoretti,
**"Preparation and characterization of liquid crystalline single-polymer short-fibres composites."**,
XX Convegno Italiano di Scienza e Tecnologia delle Macromolecole. (Oral Presentation).
Terni, Italy - 09/2011;

Medeiros Araujo, T., A. L. Yarin and A. Pegoretti
**"Single polymer micro- and nano- composites."**,
Sao Carlos Advanced School on Materials Science and Engineering. (Poster).
Sao Carlos, Brazil – 03/2012;

Medeiros Araujo T. and A. Pegoretti,
**"Liquid crystalline single-polymer short-fibres composites."**,
15TH European Conference On Composite Materials. (Oral Presentation).
Venice, Italy - 06/2012;

Medeiros Araujo, T., S. Sinha-Ray, A. Pegoretti and A. L. Yarin,
**"*Electrospinning of a blend of a liquid crystalline polymer with poly(ethylene oxide): Vectran® nanofiber mats and their mechanical properties.*"**,
European Polymer Congress – EPF 2013. (Poster)
Pisa, Italy – 06/2013;

Merlini C., T. Medeiros Araujo, G. M. O. Barra and A. Pegoretti
**"Fabrication of conducting nanocomposites of the poly(vinylidene fluoride) with polypyrrole nanoparticles by electrospinning technique."**,
European Polymer Congress – EPF 2013. (Poster)
Pisa, Italy – 06/2013.

# ACKNOWLEDGEMENTS